

---

# PDFNet: Pointwise Dense Flow Network for Urban-Scene Segmentation

---

Venkata Satya Sai Ajay Daliparthi  
Blekinge Institute of Technology  
Karlskrona, Sweden  
veda18@student.bth.se

## Abstract

In recent years, using a deep convolutional neural network (CNN) as a feature encoder (or backbone) is the most commonly observed architectural pattern in several computer vision methods, and semantic segmentation is no exception. The two major drawbacks of this architectural pattern are: (i) the networks often fail to capture small classes such as wall, fence, pole, traffic light, traffic sign, and bicycle, which are crucial for autonomous vehicles to make accurate decisions. (ii) due to the arbitrarily increasing depth, the networks require massive labeled data and additional regularization techniques to converge and to prevent the risk of over-fitting, respectively. While regularization techniques come at minimal cost, the collection of labeled data is an expensive and laborious process. In this work, we address these two drawbacks by proposing a novel lightweight architecture named point-wise dense flow network (PDFNet). In PDFNet, we employ dense, residual, and multiple shortcut connections to allow a smooth gradient flow to all parts of the network. The extensive experiments on Cityscapes and CamVid benchmarks demonstrate that our method significantly outperforms baselines in capturing small classes and in few-data regimes. Moreover, our method achieves considerable performance in classifying out-of-the training distribution samples, evaluated on Cityscapes to KITTI dataset.

## 1 Introduction

Semantic segmentation is a fundamental computer vision task in fields such as autonomous driving and robotic navigation. The pioneering work *fully convolutional network* (FCN) [1] illustrated that the image classification networks can be adopted for semantic segmentation. Several works further improved the FCN [1] architecture and have proven to be successful in diverse segmentation benchmarks.

However, due to the repeated convolutional and pooling operations, the final layers of the deep CNNs cannot fully capture the contextual information regarding various objects in the input image. Earlier works such as FCN [1] introduced skip-connections from different stages of the network to recover the lost information. The encoder-decoder networks such as DeconvNet [2], SegNet [3], and U-Net [4] learned the up-sampling process through a decoder network. Recent works [5, 6] replaced the decoder network with a simple feature map interpolation method and mainly focused on exploiting contextual information through multi-scale context [7, 6, 8, 9, 5], relational context [10–15], and boundary context modules [16–21].

Therefore, the current semantic segmentation networks pipeline can be viewed as: (1) the backbone network, (2) context encoding modules, and (3) feature map interpolation.

The backbone network is used to extract features from the input image and context modules are applied on top of those extracted features. Finally, the feature map is interpolated to match the input image resolution.

In 2015, ResNets [22] arbitrarily increased the depth of the networks up to 150+ layers and achieved state-of-the-art performance on several vision benchmarks. Since then, the deeper networks such as ResNet [22], DenseNet [23], and Inception [24] became the de-facto backbone choice for several vision methods, and semantic segmentation is no exception. The two main drawbacks of using deeper backbone networks are:

(i) On urban driving scene benchmarks, the networks often fail to capture the small classes such as wall, fence, pole, traffic light, traffic sign, and bicycle. Accurately classifying the small classes is crucial for autonomous vehicles to better understand the surroundings and to make accurate decisions. Several existing methods [16–21] exploited boundary information to refine output. However, they mainly focus on overall edge errors rather than performance on small classes.

(ii) Due to the arbitrarily increasing depth, the networks often require a massive amount of labeled data and additional regularization techniques to converge and to prevent the risk of over-fitting, respectively. While regularization techniques come at minimal cost, the collection of labeled data is an expensive and time-consuming process. Due to this reason, the U-Net [4] architecture is still exploited in several medical image segmentation methods [25].

In this work, we address the formerly mentioned drawbacks by designing a novel lightweight architecture named *point-wise dense flow network* (PDFNet). In PDFNet, we combine both the dense and residual connections to allow a smooth flow of gradient to all parts of the network. Furthermore, we attempt to investigate the architectural bottleneck limiting the performance on few data samples and small classes by proposing “the strided convolution hypothesis.”

We conduct extensive experiments on Cityscapes and CamVid benchmarks to evaluate our method and our hypothesis. The empirical results show that our PDFNet significantly outperforms baselines on, (i) accurately labeling small classes that appear in the urban driving scenario, and (ii) dealing with few data samples.

Moreover, the empirical results illustrate that our strided convolution hypothesis might be valid in few-data regimes. In other words, replacing the strided Conv with regular Conv in the first layer of the network might improve the performance on few data samples.

Additionally, we show that our networks achieve considerable out-of-training distribution performance from Cityscapes to KITTI benchmarks.

## 2 Related work

### 2.1 Encoder-decoder methods

The encoder-decoder networks such as DeconvNet [2], SegNet [3], U-Net [4], RefineNet [26, 27], and FC-DenseNet [28] employs an encoder module that encodes the semantic information by reducing spatial resolution. The spatial information lost during encoding process is generally recovered through a decoder module. The networks often uses skip-connections and pooling indices to allow information exchange between the encoder and decoder.

Several medical image segmentation methods such as DU-Net [29], MDU-Net [30], SDN [31], HyperDense-Net [32], Hybrid-DenseUNet [33], Cascaded 3D Dense-UNet [34], CUNet [35], FDU-Net [36], and Ladder-style DenseNets [37] employed dense connections [23] in encoder-decoder based architectures.

However, all the formerly mentioned encoder-decoder methods learn the up-sampling process through a decoder module that is similar to the encoder module. In contrast, the decoder module in our method only employs 1x1 Convs and feature map interpolations.

The full-resolution residual network [38] maintains an additional full-resolution stream that consists of information at the full-scale resolution. It replaces skip-connections by exchanging information from each unit in the down-sampling and up-sampling process to the full-resolution stream. In our method, we do not employ any dual-stream path and did not combine multi-scale information until the final layer.

The HRNet [39] maintains high-resolution representations throughout the network and combines information from the parallel layers. The stem in HRNet employs two 3x3 convolutional layers with stride two that reduces the size of the resulting feature map. Therefore, it only maintains representations that are four times lower than the input image resolution. On the other hand, our method maintains representations at the full-scale resolution.

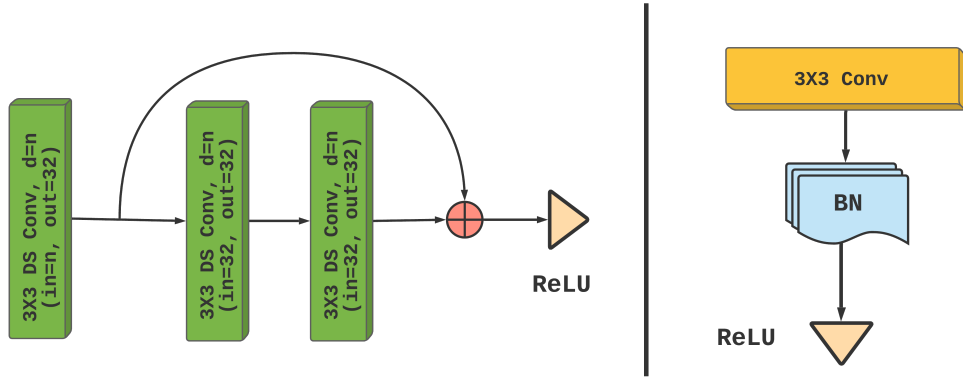


Figure 1: The glance module

## 2.2 Context encoding methods

The multi-scale context modules, such as SPP [6], ASPP [8, 9, 5], and DenseASPP [7] employs multiple parallel convolutional layers with different receptive fields to capture the multi-scale information. The relational context modules such as DANet [40], OCNNet [10], OCR [11], EncNet [12], Non-local [13], ACFNet [14], and CoCurNet [15] uses self-attention [41] approaches to compute similarities between each pixel and weights them accordingly.

In contrast, our method does not employ any of the formerly mentioned context encoding modules. On the other hand, similar to FPN [42], we use multi-scale features within the network to capture the contextual information.

## 2.3 Boundary refinement methods

The traditional methods [8, 43] employed DenseCRFs [44] to refine the segmentation output. Recent methods such as [16–19], Gated-SCNN [20], and SegFix [21] exploited boundary information through introducing refinement modules and additional streams.

The formerly mentioned boundary refinement methods only focus on overall edge error rates. In contrast, our method focuses on accurately labeling small classes.

## 2.4 Few-shot semantic segmentation (FSS)

The FSS methods employs techniques such as meta-learning (knowledge distillation) [45–49] and metric-learning (similarity learning) [50–54, 54–56] to learn from few-data samples. They involve multi-stage training and also deals with novel classes during testing.

Our method does not employ any formerly mentioned techniques to deal with few data samples and is limited to classes seen during the training. Therefore, our method is more closely related to supervised learning methods rather than few-shot learning methods.

# 3 Method

## 3.1 Pointwise dense flow network (PDFNet)

The PDFNet architecture consists of three basic building blocks. They are (i) the glance module, (ii) the  $1 \times 1$  Conv layer, and (iii) the average pooling layer.

The glance module consists of three  $3 \times 3$  dilated depth-wise separable Convs with the same dilation rate and a residual connection in between, as shown in Figure 1.

The purpose of the glance module is to explore new features and it is only employed in the encoder module. It accepts any arbitrary number of input filters and always returns 32 filters as output.

The networks such as VGG [57] ( $3 \times 3$  Convs), Inception [58] ( $3 \times 3$ ,  $5 \times 5$ ,  $7 \times 7$  Convs  $\approx 3 \times 3$  Convs with

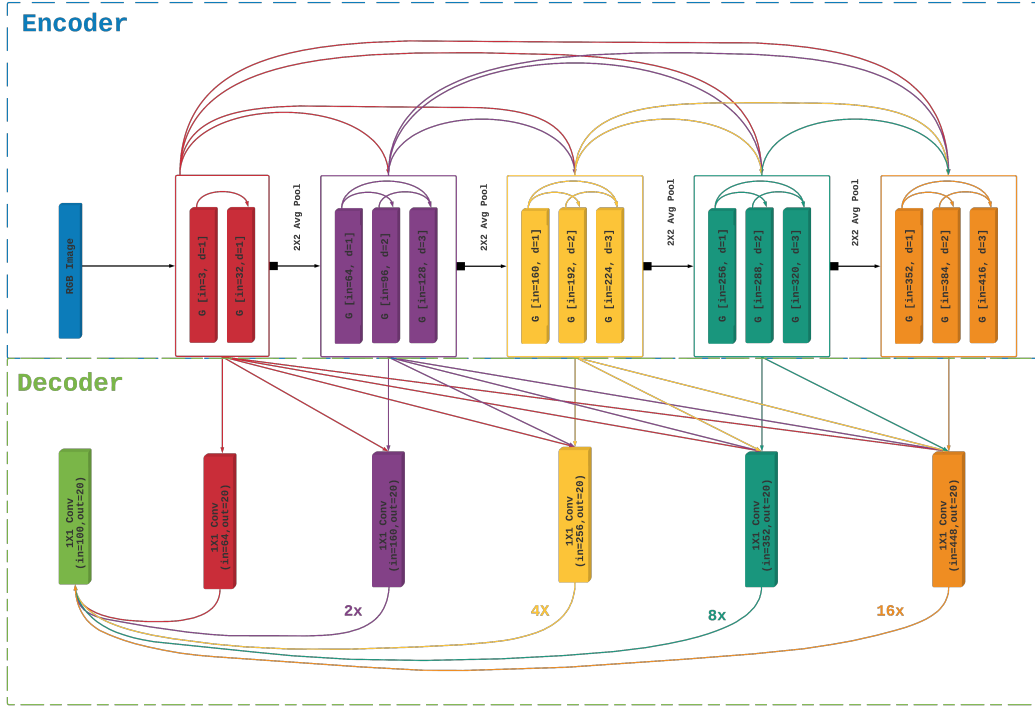


Figure 2: The PDFNet3 architecture (best viewed in color)

dilation rate = 1, 2, 3), ResNet [22] (residual connection), and Xception [59] (depth-wise separable Convs [60]) inspire the design choices of the glance module.

For a given feature map, we employ 1x1 Conv layers [61] and average pooling layers to reduce filter dimensions and spatial resolution, respectively.

Except for the last 1x1 Conv layer that returns final output, every Conv layer in the PDFNet is followed by a batch normalization [62] and a ReLU [63] activation layer.

In Figure 2, we present the PDFNet3 architecture that consists of an encoder and decoder.

At the encoder, every layer receives its preceding layers output as input through dense connections [23]<sup>1</sup>. At the first stage, we pass the RGB input image through the first glance module<sup>2</sup> and pass the resulting output (with 32 filters) through the second glance module. Then, we concatenate the resulting outputs and name it  $S_1 \Rightarrow (32 + 32 = 64)$ . Here, we pass  $S_1$  through an average pooling layer to reduce the spatial resolution by half. Then, we pass the pooled  $S_1$  through the second stage of the network that consists of three glance modules with different dilation rates ( $d = 1, 2, 3$ ). The second stage of the network returns  $S_2$  with 160 filters (64 from stage one + 96 from stage two). The same process repeats for another three stages and at every stage the networks stores the resulting outputs ( $S_1(64)$ ,  $S_2(160)$ ,  $S_3(256)$ ,  $S_4(352)$ , and  $S_5(448)$ ).

At the decoder, we pass encoder outputs through an individual 1x1 Conv layer that reduces the number of filters to 20 ( $S_1(20)$ ,  $S_2(20)$ ,  $S_3(20)$ ,  $S_4(20)$ , and  $S_5(20)$ )<sup>3</sup>. Then, we bi-linearly interpolate the outputs from the last four stages ( $S_2$ ,  $S_3$ ,  $S_4$ , and  $S_5$ ) to match with the resolution of the first stage

<sup>1</sup>The encoder connections in the PDFNet are similar to the full dense connectivity pattern introduced in CondenseNet [64]. However, the basic building block of [64] consists of a learnable group 1x1 Conv layer (to prune the incoming filters), a shuffling layer, and multiple 3x3 group Conv layers, which is entirely different from our glance module.

<sup>2</sup>For the first Conv layer in the first glance module, we replace the depth-wise separable Conv with a regular Conv layer.

<sup>3</sup>This is closely related to FPN [42], which also uses multi-scale information within the network. However, FPN [42] omits the first Conv layer features and learns 256 filters from the last three stages, which are further refined with multiple 3x3 Conv layers. On the other hand, our method learns only 20 filters from each stage and does not employ additional 3x3 Conv layers to refine them, which allows us to operate on the full-scale resolution.

( $S_1$ ). After that, we concatenate the five-stage outputs ( $20 * 5 = 100$ ) and pass them through a  $1 \times 1$  Conv layer, which takes in 100 filters and returns 20 filters, that is the final output of the network. In PDFNet, every layer receives gradient through successive layers (see the shortcut connections in Figure 2). For instance, the output of first glance module  $S_1$  contributes to every stage in the decoder. For any PDFNet variant, the depth of the first two stages remains unchanged. However, for PDFNet6, PDFNet9, and PDFNet12, the number of glance modules in the last three stages are increased to six, nine, and twelve, respectively.

### 3.2 The strided convolution hypothesis

In recent years, the most commonly observed architectural pattern in deep CNNs such as ResNet [22], and DenseNet [23] is to apply a Conv layer with stride two on the input image, which reduces the size of the resulting feature map by half. In the existing literature, this is also referred to as “*the stem module*”.

To the best of our knowledge, the stride in the stem module is due to the computational complexity of operating on the full-scale resolution.

While adopting deep CNNs for the high-level tasks such as semantic segmentation, many methods [8, 9, 5]<sup>4</sup> often replaced the Conv layers in the last stage with dilated Convs, to increase the receptive field while maintaining the spatial resolution. However, the stride in the stem module remains unchanged in almost every method.

Here, we observe that, while the input and output resolutions are equal in semantic segmentation, many methods are not capturing representations at the full-scale resolution.

Therefore, we hypothesize that “*the stride two in the first Conv layer might be the bottleneck limiting the performance on small classes and few data samples*”, i.e., *the strided convolution hypothesis*

To validate our hypothesis, we design four PDFNet variants named PDFNet3-2S, PDFNet6-2S, PDFNet9-2S, and PDFNet12-2S, by removing the first stage and employing stride two in the first Conv layer in the networks PDFNet3, PDFNet6, PDFNet9, and PDFNet12, respectively.

On the other hand, the earlier networks such as DeconvNet [2], SegNet [3], and U-Net [4] use regular Conv in the first layer by following VGG [57], and captures representations at the full-scale resolution.

## 4 Experiments

### 4.1 Experimental setup

Framework : PyTorch 1.8 [65]

GPU: 1 X NVIDIA Tesla P-100 (16 GB VRAM)

Epochs : 180

Batch size : 2

Criterion : Pixel-wise cross-entropy loss

Learning rate scheduler : ReduceLROnPlateau (decrease factor = 0.5 and patience = 20 epochs) with an initial learning rate of  $1e - 06$ .

Optimizer : Stochastic gradient descent [66] with Nesterov momentum <sup>5</sup> [70].

Random seed : We set random seed 42 as argument in the function `torch.utils.data.RandomSplit` to ensure that the data splits are reproducible.

Pre-processing: We normalize all the images with mean and standard deviation values of [71] and did not use any data augmentation techniques.

Baselines : We use the open-source implementations for networks DeepLabV3+ (ResNet-101) [72], DeepLabV3 (DenseNet-161) [73], HRNet-V2 [74], and U-Net [75]. We import DeeplabV3+ with encoder networks such as ResNet [22], MobileNet-V2 [67], ResNext [76], EfficientNet [68], and RegNet [69] from the segmentation models library [77]<sup>6</sup>.

<sup>4</sup>Some methods replaced the first  $7 \times 7$  Conv layer in the ResNet [22] with a  $3 \times 3$  Conv layer.

<sup>5</sup>For all the baselines, we set momentum value to 0.9 by following [5, 23, 22, 67–69, 4, 39]. In contrast, we set momentum value to 0.7 for all the variants of PDFNet. In our preliminary experiments, we observe that the training of PDFNet is unstable with 0.9 momentum. We hypothesize that this phenomenon is due to the small size of PDFNet compared to baseline networks.

<sup>6</sup>In all the experiments, we use ImageNet [71] pre-trained weights for DeepLabV3+ [5] with backbone networks ResNet-101 [22], DenseNet-161 [23], HRNet-V2 [39], EfficientNet-b6 [68], and RegNetY-80 [69].

Method	road	sidewalk	building	wall	fence	pole	traffic light	traffic sign	vegetation	terrain	sky	person	rider	car	truck	bus	train	motorcycle	bicycle	Average
ResNet101 [22]	95.0	66.1	81.9	15.0	13.5	26.7	20.7	29.5	86.7	55.4	89.3	48.5	6.3	85.5	6.8	26.1	19.0	9.8	32.0	42.8
DenseNet161 [23]	94.8	64.5	81.3	20.1	13.0	15.8	15.6	28.7	84.6	<b>58.7</b>	86.1	44.1	0.6	84.7	17.0	19.7	23.1	4.3	31.4	41.5
HRNet-V2 [39]	94.9	68.6	84.2	24.0	24.5	39.0	23.2	42.3	86.9	51.5	90.2	55.6	15.3	86.1	19.9	36.1	21.2	2.2	46.1	48.0
U-Net [4]	94.9	69.4	85.3	27.3	28.7	41.0	32.2	49.0	88.6	46.3	90.4	59.1	14.5	86.5	12.4	28.4	15.5	10.9	55.6	49.3
PDFNet3	94.7	71.3	85.9	31.8	37.9	44.1	36.4	52.1	87.9	49.6	91.4	55.1	13.5	86.0	25.4	43.9	20.0	9.4	52.4	52.0
PDFNet6	<b>95.5</b>	72.3	86.0	34.4	39.6	43.4	37.1	51.9	88.3	52.0	91.4	58.6	23.3	87.1	35.4	47.8	25.4	11.2	56.8	54.6
PDFNet9	94.8	<b>72.9</b>	85.8	34.0	39.7	41.7	<b>39.1</b>	<b>55.7</b>	88.0	51.5	91.4	55.8	16.1	86.9	23.1	40.6	20.9	<b>14.9</b>	53.8	53.0
PDFNet12	94.6	72.1	<b>86.5</b>	<b>36.2</b>	<b>39.8</b>	<b>44.8</b>	36.0	54.7	<b>88.8</b>	53.1	<b>91.7</b>	<b>59.6</b>	24.8	<b>88.0</b>	35.0	<b>52.5</b>	18.4	9.6	<b>57.7</b>	<b>54.9</b>
PDFNet3-2S	95.0	69.4	84.4	25.4	35.0	38.8	23.5	42.8	87.1	48.5	90.0	50.8	1.9	83.9	19.0	39.6	24.9	8.5	50.3	48.4
PDFNet6-2S	94.7	69.2	85.0	33.9	33.1	38.7	28.5	47.9	87.5	51.0	91.1	54.4	14.4	85.3	21.0	33.6	13.8	8.2	51.6	49.6
PDFNet9-2S	95.1	71.2	85.4	30.9	32.6	41.1	31.0	47.9	87.5	53.3	90.9	58.2	<b>25.5</b>	86.6	<b>37.5</b>	50.2	<b>31.5</b>	12.1	52.2	53.7
PDFNet12-2S	95.2	72.3	85.6	<b>36.2</b>	32.9	42.2	32.5	49.1	87.8	52.6	90.8	57.6	20.4	86.4	33.2	45.5	19.0	14.1	52.3	52.9

Table 1: Class-wise results of the Cityscapes baseline experiments evaluated on the validation set

## 4.2 Experiments on Cityscapes

### 4.2.1 Dataset

The Cityscapes [78] pixel-level labeling dataset consists of 5,000 high-resolution images finely annotated into 35 classes. Which are further divided into 2,975/500/1,525 images for training, validation, and testing, respectively. We convert 35 classes into 20 classes (including background) and resize the images from 1024x2048 to 512x1024.

### 4.2.2 Baseline Experiments

To evaluate the performance of our method on different classes that appear in an urban driving scene, we conduct baseline experiments on the entire Cityscapes dataset. We select DeepLabV3+ (ResNet-101) [22], DeepLabV3 (DenseNet-161) [23], HRNet-V2 [39], and U-Net [4] as the baselines, along with four PDFNet and PDFNet-2S variants.

In Table 1, we present mean class-wise IoU results of the networks evaluated on the val set. From Table 1, we observe and hypothesize the following:

(i) Every PDFNet variant outperforms all other baseline networks, and PDFNet12 achieves top performance (54.9).

(ii) Within the baseline networks, U-Net [4] has shown top performance (49.3), followed by HRNet-V2 [39] (48.0).

(iii) Comparing ResNet-101 [22] (42.8), DenseNet-161 [23] (41.5), and HRNet-V2 [39] (48.0). The HRNet-V2 [39] outperformed other networks in classes such as pole, traffic sign, person, rider, bus, and bicycle. These performance gains of HRNet-V2 [39] are might be due to the maintained high-resolution representations.

(iv) Comparing HRNet-V2 [79] (48.0) and U-Net [4] (49.3). The HRNet-V2 [79] employs two strided Convs in the stem module, which results in a feature map that is four times smaller than the input image. On the other hand, U-Net [4] captures 64 filters at the full-scale resolution before reducing the spatial resolution. The U-Net [4] outperforms HRNet-V2 [39] in classes (such as wall, fence, traffic light, traffic sign, person, motorcycle, and bicycle), and HRNet-V2 [39] outperforms U-Net [4] in classes (such as terrain, truck, bus, and train). We attribute the former behavior of U-Net [4] to the captured full-scale representations, and the latter behavior of HRNet-V2 [39] to the depth on low-resolution feature maps.

(v) Comparing U-Net [4] (49.3) and PDFNet variants [PDFNet12 (54.9), PDFNet9 (53.0), PDFNet6 (54.6), and PDFNet3 (52.0)]. Even though, both the networks capture full-scale representations before reducing the spatial resolution. The PDFNet variants outperform U-Net [4] in classes such as wall, fence, pole, traffic light, traffic sign, terrain, rider, truck, bus, and train. We attribute this behavior of PDF-Net to the dense connections, simple decoder, and network design choices.

(vi) Comparing PDFNet3 (52.0) and PDFNet-2S variants [PDFNet12-2S (52.9), PDFNet9-2S (53.7), PDFNet6-2S (49.6), and PDFNet3-2S (48.4)]. The PDFNet3 outperformed all the PDFNet-2S variants in classes such as pole, traffic light, and traffic sign.

(vii) Despite the fact that PDFNet-2S variants do not capture representations at full-scale resolution, their performance on small classes is almost similar to U-Net [4].

From the above observations, we found no clear evidence to support our strided convolution hypothesis (3.2), and found that PDFNet variants significantly outperforms baselines on small classes.

Because in the existing literature, it is mentioned that these methods used an ImageNet [71] pre-trained network as a feature encoder and reported results with pre-trained weights only.

Backbone	$T_{1487}$	$T_{743}$	$T_{371}$	$T_{185}$	$T_{92}$	$T_{avg}$	Param(M)	GFLOPS
ResNet-18 [22]	42.6	35.6	27.9	22.4	21.0	29.9	12.3	36.8
MobileNet-V2 [67]	38.5	32.2	30.6	22.5	19.2	28.6	4.4	12.3
EfficientNet-b1 [68]	37.8	32.5	26.9	24.6	19.8	28.3	7.4	4.6
RegNetY-08 [69]	28.5	31.9	29.4	27.4	22.1	27.9	7.0	17.2
ResNet-101 [22]	29.3	28.8	28.6	21.6	19.4	25.5	59.3	177.8
DenseNet-161 [23]	33.3	30.1	26.0	24.9	20.8	27.0	43.2	129.4
HRNet-V2 [39]	27.8	18.8	23.3	18.3	15.4	20.7	65.9	187.8
U-Net[4]	42.8	34.2	30.2	27.8	25.0	32.0	31.0	387.1
PDFNet3	47.1	42.9	39.9	34.7	29.7	38.9	0.2	8.0
PDFNet6	49.6	43.2	39.1	<b>35.8</b>	<b>30.5</b>	39.6	0.4	10.3
PDFNet9	48.8	44.9	<b>40.0</b>	34.1	29.3	39.4	0.8	13.5
PDFNet12	<b>50.8</b>	<b>46.6</b>	38.5	33.8	30.3	<b>40.0</b>	1.2	17.5
PDFNet3-2S	44.7	40.0	34.0	33.4	29.9	36.4	<b>0.1</b>	<b>2.7</b>
PDFNet6-2S	46.9	40.5	38.2	32.6	24.3	36.5	0.3	4.5
PDFNet9-2S	47.3	43.7	35.9	32.9	27.6	37.5	0.7	7.5
PDFNet12-2S	46.0	40.1	36.9	31.4	28.0	36.5	1.1	11.1

Table 2: Cityscapes data ablation experiments evaluated on the validation set

### 4.2.3 Data ablation study

To evaluate the performance of our method on few data samples, we conduct a data ablation study on the Cityscapes dataset. The size of the baseline networks ResNet-101 [22] (59.3M), DenseNet-161 [23] (43.2M), HRNet-V2 [39] (65.9M), and U-Net [4] (31.0M) is huge compared to PDFNet variants (PDFNet12 (1.2M), PDFNet9 (758K), PDFNet6 (405K), and PDFNet3 (164K)).

The less size of networks might strongly benefit while training on few data samples. Hence, we also add the DeeplabV3+ [5] with several light-weight encoder networks such as ResNet-18 [22], MobileNet-V2 [67], EfficientNet-b1 [68], and RegNetY-08 [69] in this data ablation study along with PDFNet-2S variants.

We train each network on five different subsets of training data  $T_{1487}$ ,  $T_{743}$ ,  $T_{371}$ ,  $T_{185}$ , and  $T_{92}$  (the number in suffix represents the training samples in each set) by using the same val set. In Table 2, we present mean IoU results of the networks evaluated on validation set, parameters, and GFLOPs [80] (calculated with an input resolution of  $1x512x1024x3$ ). From Table 2, we observe that:

- (i) Every PDFNet and PDFNet-2S variant outperforms the baseline networks by a considerable margin <sup>7</sup> and PDFNet12 achieves the top average IoU score (40.0).
- (ii) Every PDFNet-2S variant under-performed while compared to every PDFNet variant.
- (iii) The PDFNet3-2S requires fewer parameters, and GFLOPs than other networks.
- (iv) Even though the size of U-Net (31.0M) [4] is larger than the lightweight encoder networks (ResNet-18 (12.3M) [22], MobileNet-V2 (4.4M) [67], EfficientNet-b1 (7.4M) [68], and RegNetY-08 (7.0M) [69]). The U-Net [4] still outperforms other baseline networks in the average IOU score.

Here, we observe that the performance of the networks trained on few data samples correlates more with the selected architecture rather than network size.

From the above, we found some evidence (ii) to support our strided convolution hypothesis (3.2) in this few data regime.

Additionally, In Table 1, even though the M.IoU score difference between HRNet-V2 [39] and U-Net [4] is only 1.3, in Table 2 its is 11.3 ( $T_{Avg}$ ). This hints that performance of HRNet-V2 [39] might highly depend upon the training data.

<sup>7</sup>Here, one might argue that the network size of the PDFNet variants is very less compared to any baseline network. We provide additional experiments in the supplementary material, to show that the performance gains of PDFNet on few data samples are due to the proposed architecture and not due to the less size of the network.

Backbone	$T_{367}$		$T_{183}$		$T_{91}$		$T_{avg}$		Param(M)	GFLOPS
	Val	Test	Val	Test	Val	Test	Val	Test		
ResNet-18 [22]	83.3	64.9	79.7	63.7	70.0	56.6	77.7	61.7	12.3	12.4
EfficientNet-b1 [68]	<b>84.4</b>	<b>68.4</b>	75.0	61.3	77.0	58.8	78.8	62.8	7.4	1.5
RegNetY-08 [69]	80.4	64.3	77.7	61.4	70.9	57.8	76.3	61.2	7.0	5.8
MobileNet-V2 [67]	80.8	63.9	77.3	56.1	64.4	57.0	74.2	59.0	4.4	4.1
PDFNet3	83.3	67.5	<b>82.6</b>	63.0	<b>80.7</b>	<b>64.5</b>	<b>82.2</b>	65.0	0.2	2.3
PDFNet3-2S	83.1	67.4	81.8	61.7	78.6	62.0	81.2	63.7	<b>0.1</b>	<b>0.8</b>
PDFNet6	84.0	68.0	82.2	<b>66.8</b>	80.2	62.5	82.1	<b>65.8</b>	0.4	3.0
PDFNet6-2S	82.2	65.9	80.5	64.0	77.9	59.9	80.2	63.3	0.3	1.4
ResNet-50 [22]	78.6	61.6	79.6	60.3	78.3	55.9	78.8	59.3	26.7	25.0
EfficientNet-b4 [68]	82.7	64.1	77.7	62.2	75.6	60.5	78.7	62.3	18.6	<b>1.7</b>
RegNetY-40 [69]	80.8	63.8	76.4	61.0	74.9	59.2	77.4	61.3	21.5	18.8
ResNext-50 [76]	80.1	62.6	81.0	63.9	77.9	59.9	79.7	62.1	26.2	25.0
U-Net [4]	83.0	<b>69.5</b>	78.0	62.8	76.8	61.6	79.3	64.6	31.0	130.0
PDFNet9	<b>83.8</b>	67.4	<b>83.5</b>	<b>66.0</b>	<b>82.0</b>	<b>64.7</b>	<b>83.1</b>	<b>66.0</b>	0.7	4.1
PDFNet9-2S	82.5	66.0	80.9	64.4	78.1	61.7	80.5	64.0	<b>0.6</b>	2.4
ResNet-101 [22]	81.6	63.8	75.6	56.4	70.1	55.7	75.8	58.6	59.3	59.9
EfficientNet-b6 [68]	80.6	65.0	80.3	57.8	77.4	60.4	79.4	61.0	42.0	<b>1.9</b>
RegNetY-80 [69]	78.5	62.0	78.2	63.8	66.2	53.8	74.3	59.9	40.3	34.4
DenseNet-161 [23]	77.8	58.6	75.5	57.7	73.0	53.8	75.4	56.7	43.2	43.6
HRNet-V2 [39]	81.1	63.6	79.1	62.9	72.9	55.0	77.7	60.5	65.9	63.5
PDFNet12	<b>84.3</b>	<b>68.0</b>	<b>82.0</b>	<b>67.0</b>	<b>80.9</b>	<b>60.9</b>	<b>82.4</b>	<b>65.3</b>	1.2	5.4
PDFNet12-2S	83.1	65.5	80.9	62.4	79.5	60.2	81.2	62.7	<b>1.1</b>	3.6

Table 3: Camvid baseline experiments evaluated on the validation and the test sets

### 4.3 Experiments on CamVid

#### 4.3.1 Dataset

The CamVid dataset [81] for semantic segmentation consists of 700 images divided into three sets 367 training, 101 validation, and 233 testing. By following [3, 82], we use 12 classes (including background) and resize the images from 720x960 to 368x480.

#### 4.3.2 Baseline experiments

We conduct baseline experiments on CamVid dataset using three different sets, divided according to the networks size.

Set-1 consists of DeeplabV3+ [5] with encoders networks, Resnet-18 [22], EfficientNet-b1 [68], RegNetY-08 [69], MobileNet-V2 [67], PDFNet3, PDFNet3-2S, PDFNet6, and PDFNet6-2S.

Set-2 consists of DeeplabV3+ [5] with encoder networks, Resnet-50 [22], EfficientNet-b4 [68], RegNetY-40 [69], ResNext-50 [76], U-Net, PDFNet9, and PDFNet9-2S.

Set-3 consists of DeeplabV3+ [5] with encoder networks, Resnet-101 [22], EfficientNet-b6 [68], RegNetY-80 [69], DeepLabV3 (DenseNet-161 [23]), HRNet-V2, PDFNet12, and PDFNet12-2S.

We train each network on three subsets of the training set ( $T_{367}$ ,  $T_{183}$ , and  $T_{91}$ ) by using the same validation set and test set. In Table 3, we present M.IoU score on validation set, test test, parameters, and GFLOPS [80] (calculated with an input resolution of 1x368x480x3).

From Table 3, we observe that:

(i) In all three sets, PDFNet variants outperforms other networks in  $T_{183}$ ,  $T_{91}$  and  $T_{Avg}$ , and require fewer parameters and GFLOPs.

(ii) With in the networks trained on subset  $T_{367}$ , EfficientNet-b1 [68] in Set-1, U-Net [4] in Set-2, and PDFNet12 in Set-3 achieves top performance.

(iii) In all three sets, PDFNet variants significantly outperforms PDFNet-2S variants in  $T_{183}$ ,  $T_{91}$  and  $T_{Avg}$ .

From the above observations, we found a similar pattern as Table 2 that supports our strided convolution hypothesis (3.2) in the less data regimes.



Backbone	$T_{1487}$		$T_{743}$		$T_{371}$		$T_{185}$		$T_{92}$		$T_{avg}$	
	Class	Cat	Class	Cat	Class	Cat	Class	Cat	Class	Cat	Class	Cat
ResNet-18 [22]	15.1	30.8	12.0	27.0	10.5	25.2	7.9	20.4	9.8	24.7	11.1	25.6
MobileNet-V2 [67]	<b>21.6</b>	<b>42.6</b>	17.2	<b>38.5</b>	15.8	<b>37.6</b>	13.2	30.9	13.6	32.9	16.3	36.6
EfficientNet-b1 [68]	19.5	42.2	15.2	36.5	14.2	34.2	8.1	20.9	6.1	15.4	12.6	29.8
RegNetY-08 [69]	10.8	26.6	12.9	30.4	12.6	29.8	11.5	27.6	10.1	24.0	11.6	27.7
ResNet-101 [22]	12.0	26.4	11.6	28.3	8.8	21.3	8.8	22.3	7.5	19.0	9.7	23.5
DenseNet-161 [23]	10.5	24.0	8.0	19.8	9.7	23.3	11.2	27.0	8.4	21.7	9.6	23.2
HRNet-V2 [39]	6.9	16.8	8.1	19.9	7.9	20.6	9.3	24.0	11.2	29.5	8.7	22.2
U-Net [4]	14.1	31.8	12.8	30.5	9.3	23.2	9.0	22.6	7.9	20.6	10.6	25.7
PDFNet3	17.2	36.8	13.0	28.3	16.0	34.4	12.3	28.4	15.0	33.0	14.7	32.2
PDFNet6	18.7	38.2	15.2	32.5	15.2	34.4	14.4	30.8	16.4	35.7	16.0	34.3
PDFNet9	20.9	39.2	<b>17.3</b>	35.6	15.5	33.4	14.4	32.2	14.6	32.9	16.5	34.7
PDFNet12	18.3	37.3	17.1	35.5	<b>17.8</b>	36.7	<b>16.0</b>	<b>36.7</b>	<b>17.4</b>	<b>40.0</b>	<b>17.3</b>	<b>37.2</b>
PDFNet3-2S	14.3	29.5	12.1	27.4	13.3	30.5	12.7	29.4	14.3	32.2	13.4	29.8
PDFNet6-2S	19.4	36.7	14.8	33.2	14.5	32.5	13.9	30.5	13.8	32.6	15.8	33.1
PDFNet9-2S	16.7	35.1	15.4	34.6	16.9	37.4	14.5	32.9	14.1	33.1	15.5	34.6
PDFNet12-2S	18.6	39.1	16.3	34.6	16.9	36.5	14.6	34.7	13.4	32.3	16.0	35.4

Table 4: Cityscapes data ablation experiments evaluated on the KITTI training set

## 4.4 Generalization on KITTI

### 4.4.1 Dataset

The KITTI semantic segmentation dataset [83] consists of 400 images divided into 200 training and 200 testing sets.

### 4.4.2 Cityscapes to KITTI

Since the data format and metrics of KITTI dataset are consistent with Cityscapes [83], we use it to evaluate the out-of-training distribution performance of the networks trained on Cityscapes dataset. In Table 4, we provide mean class and category IoU scores of the networks from Cityscapes data ablation study evaluated on KITTI training set. From Table 4, we observe that:

- (i) The PDFNet12 outperforms other networks in average class and category IoU score.
- (ii) The PDFNet-2S variants performed almost similar to PDFNet variants.
- (iii) Within the baseline networks, the MobileNet-V2 [67] shown considerable generalization performance.

Here, we hypothesize that the generalization performance of PDFNet variants is due to the captured generalized features than dataset-specific features.

## 5 Conclusion

- (i) In this work, we introduced a novel lightweight framework for urban scene segmentation named PDFNet to deal with small classes and few data samples.

The extensive experiments on Cityscapes and CamVid benchmarks demonstrate the effectiveness of our method compared to baselines. Moreover, our method achieves considerable generalization performance in labeling out-of-training distribution samples.

- (ii) In this work, we found that replacing the strided Conv with regular Conv in the first layer (or the stem module) of the networks might help in dealing with few data samples.

In other words, we observe that our strided convolution hypothesis (3.2) is valid in the few data regimes.

The (i) and (ii) are the main contributions of this work.

Improving the performance on small classes, few data samples and real-time applicability on several hardware platforms will be studied in future work.

## References

- [1] Jonathan Long, Evan Shelhamer, and Trevor Darrell. Fully convolutional networks for semantic segmentation. In *Proceedings of the IEEE conference on computer vision and pattern recognition*, pages 3431–3440, 2015.

- [2] Hyeonwoo Noh, Seunghoon Hong, and Bohyung Han. Learning deconvolution network for semantic segmentation. In *Proceedings of the IEEE international conference on computer vision*, pages 1520–1528, 2015.
- [3] Vijay Badrinarayanan, Alex Kendall, and Roberto Cipolla. Segnet: A deep convolutional encoder-decoder architecture for image segmentation. *IEEE transactions on pattern analysis and machine intelligence*, 39(12):2481–2495, 2017.
- [4] Olaf Ronneberger, Philipp Fischer, and Thomas Brox. U-net: Convolutional networks for biomedical image segmentation. In *International Conference on Medical image computing and computer-assisted intervention*, pages 234–241. Springer, 2015.
- [5] Liang-Chieh Chen, Yukun Zhu, George Papandreou, Florian Schroff, and Hartwig Adam. Encoder-decoder with atrous separable convolution for semantic image segmentation. In *Proceedings of the European conference on computer vision (ECCV)*, pages 801–818, 2018.
- [6] Hengshuang Zhao, Jianping Shi, Xiaojuan Qi, Xiaogang Wang, and Jiaya Jia. Pyramid scene parsing network. In *Proceedings of the IEEE conference on computer vision and pattern recognition*, pages 2881–2890, 2017.
- [7] Maoge Yang, Kun Yu, Chi Zhang, Zhiwei Li, and Kuiyuan Yang. Denselaspp for semantic segmentation in street scenes. In *2018 IEEE/CVF Conference on Computer Vision and Pattern Recognition*, pages 3684–3692, 2018.
- [8] Liang-Chieh Chen, George Papandreou, Iasonas Kokkinos, Kevin Murphy, and Alan L. Yuille. Deeplab: Semantic image segmentation with deep convolutional nets, atrous convolution, and fully connected crfs. *IEEE Transactions on Pattern Analysis and Machine Intelligence*, 40(4):834–848, 2018.
- [9] Liang-Chieh Chen, George Papandreou, Florian Schroff, and Hartwig Adam. Rethinking atrous convolution for semantic image segmentation. *CoRR*, abs/1706.05587, 2017.
- [10] Yuhui Yuan and Jingdong Wang. Ocnet: Object context network for scene parsing. *CoRR*, abs/1809.00916, 2018.
- [11] Yuhui Yuan, Xilin Chen, and Jingdong Wang. Object-contextual representations for semantic segmentation. In Andrea Vedaldi, Horst Bischof, Thomas Brox, and Jan-Michael Frahm, editors, *Computer Vision – ECCV 2020*, pages 173–190, Cham, 2020. Springer International Publishing.
- [12] Hang Zhang, Kristin Dana, Jianping Shi, Zhongyue Zhang, Xiaogang Wang, Amrbrish Tyagi, and Amit Agrawal. Context encoding for semantic segmentation. In *The IEEE Conference on Computer Vision and Pattern Recognition (CVPR)*, June 2018.
- [13] Xiaolong Wang, Ross Girshick, Abhinav Gupta, and Kaiming He. Non-local neural networks. In *2018 IEEE/CVF Conference on Computer Vision and Pattern Recognition*, pages 7794–7803, 2018.
- [14] Fan Zhang, Yanqin Chen, Zhihang Li, Zhibin Hong, Jingtuo Liu, Feifei Ma, Junyu Han, and Errui Ding. Acfnets: Attentional class feature network for semantic segmentation. In *2019 IEEE/CVF International Conference on Computer Vision (ICCV)*, pages 6797–6806, 2019.
- [15] Hang Zhang, Han Zhang, Chenguang Wang, and Junyuan Xie. Co-occurrent features in semantic segmentation. In *2019 IEEE/CVF Conference on Computer Vision and Pattern Recognition (CVPR)*, pages 548–557, 2019.
- [16] Gedas Bertasius, Jianbo Shi, and Lorenzo Torresani. High-for-low and low-for-high: Efficient boundary detection from deep object features and its applications to high-level vision. In *Proceedings of the IEEE International Conference on Computer Vision (ICCV)*, December 2015.
- [17] Liang-Chieh Chen, Jonathan T Barron, George Papandreou, Kevin Murphy, and Alan L Yuille. Semantic image segmentation with task-specific edge detection using cnns and a discriminatively trained domain transform. In *CVPR*, 2016.

- [18] Henghui Ding, Xudong Jiang, Ai Qun Liu, Nadia Magnenat Thalmann, and Gang Wang. Boundary-aware feature propagation for scene segmentation. In *Proceedings of the IEEE/CVF International Conference on Computer Vision (ICCV)*, October 2019.
- [19] Dmitrii Marin, Zijian He, Peter Vajda, Priyam Chatterjee, Sam S. Tsai, Fei Yang, and Yuri Boykov. Efficient segmentation: Learning downsampling near semantic boundaries. In *2019 IEEE/CVF International Conference on Computer Vision, ICCV 2019, Seoul, Korea (South), October 27 - November 2, 2019*, pages 2131–2141. IEEE, 2019.
- [20] Towaki Takikawa, David Acuna, Varun Jampani, and Sanja Fidler. Gated-scnn: Gated shape cnns for semantic segmentation. *ICCV*, 2019.
- [21] Yuhui Yuan, Jingyi Xie, Xilin Chen, and Jingdong Wang. Segfix: Model-agnostic boundary refinement for segmentation. In *European Conference on Computer Vision*, pages 489–506. Springer, 2020.
- [22] Kaiming He, Xiangyu Zhang, Shaoqing Ren, and Jian Sun. Deep residual learning for image recognition. In *Proceedings of the IEEE conference on computer vision and pattern recognition*, pages 770–778, 2016.
- [23] Gao Huang, Zhuang Liu, Laurens VanDerMaaten, and KilianQ Weinberger. Densely connected convolutional networks. In *Proceedings of the IEEE conference on computer vision and pattern recognition*, pages 4700–4708, 2017.
- [24] Christian Szegedy, Sergey Ioffe, Vincent Vanhoucke, and Alexander A Alemi. Inception-v4, inception-resnet and the impact of residual connections on learning. In *Thirty-first AAAI conference on artificial intelligence*, 2017.
- [25] Nahian Siddique, Paheding Sidike, Colin Elkin, and Vijay Devabhaktuni. U-net and its variants for medical image segmentation: theory and applications. *arXiv preprint arXiv:2011.01118*, 2020.
- [26] G. Lin, A. Milan, C. Shen, and I. Reid. RefineNet: Multi-path refinement networks for high-resolution semantic segmentation. In *CVPR*, July 2017.
- [27] Guosheng Lin, Fayao Liu, Anton Milan, Chunhua Shen, and Ian Reid. Refinenet: Multi-path refinement networks for dense prediction. *IEEE Transactions on Pattern Analysis and Machine Intelligence*, 2019.
- [28] Simon Jégou, Michal Drozdal, David Vazquez, Adriana Romero, and Yoshua Bengio. The one hundred layers tiramisu: Fully convolutional densenets for semantic segmentation. In *2017 IEEE Conference on Computer Vision and Pattern Recognition Workshops (CVPRW)*, pages 1175–1183, 2017.
- [29] Zhiqiang Tang, Xi Peng, Shijie Geng, Lingfei Wu, Shaoting Zhang, and Dimitris Metaxas. Quantized densely connected u-nets for efficient landmark localization. In *Proceedings of the European Conference on Computer Vision (ECCV)*, pages 339–354, 2018.
- [30] Jiawei Zhang, Yuzhen Jin, Jilan Xu, Xiaowei Xu, and Yanchun Zhang. Mdu-net: Multi-scale densely connected u-net for biomedical image segmentation. *arXiv preprint arXiv:1812.00352*, 2018.
- [31] Jun Fu, Jing Liu, Yuhang Wang, Jin Zhou, Changyong Wang, and Hanqing Lu. Stacked deconvolutional network for semantic segmentation. *IEEE Transactions on Image Processing*, 2019.
- [32] Jose Dolz, Karthik Gopinath, Jing Yuan, Herve Lombaert, Christian Desrosiers, and Ismail Ben Ayed. Hyperdense-net: a hyper-densely connected cnn for multi-modal image segmentation. *IEEE transactions on medical imaging*, 38(5):1116–1126, 2018.
- [33] Xiaomeng Li, Hao Chen, Xiaojuan Qi, Qi Dou, Chi-Wing Fu, and Pheng-Ann Heng. H-denseunet: hybrid densely connected unet for liver and tumor segmentation from ct volumes. *IEEE transactions on medical imaging*, 37(12):2663–2674, 2018.

- [34] Mina Ghaffari, Arcot Sowmya, and Ruth Oliver. Brain tumour segmentation using cascaded 3d densely-connected u-net. *arXiv preprint arXiv:2009.07563*, 2020.
- [35] Le Dong, Ling He, Mengdie Mao, Gaipeng Kong, Xi Wu, Qianni Zhang, Xiaochun Cao, and Ebroul Izquierdo. CUNET: A compact unsupervised network for image classification. *IEEE Transactions on Multimedia*, 20(8):2012–2021, 2017.
- [36] Steven Guan, Amir A. Khan, Siddhartha Sikdar, and Parag V. Chitnis. Fully dense unet for 2-d sparse photoacoustic tomography artifact removal. *IEEE Journal of Biomedical and Health Informatics*, 24(2):568–576, 2020.
- [37] Ivan Kreso, Sinisa Segvic, and Josip Krapac. Ladder-style densenets for semantic segmentation of large natural images. In *Proceedings of the IEEE International Conference on Computer Vision Workshops*, pages 238–245, 2017.
- [38] Tobias Pohlen, Alexander Hermans, Markus Mathias, and Bastian Leibe. Full-resolution residual networks for semantic segmentation in street scenes. In *Proceedings of the IEEE Conference on Computer Vision and Pattern Recognition*, pages 4151–4160, 2017.
- [39] Ke Sun, Yang Zhao, Borui Jiang, Tianheng Cheng, Bin Xiao, Dong Liu, Yadong Mu, Xinggang Wang, Wenyu Liu, and Jingdong Wang. High-resolution representations for labeling pixels and regions. *CoRR*, abs/1904.04514, 2019.
- [40] Jun Fu, Jing Liu, Haijie Tian, Yong Li, Yongjun Bao, Zhiwei Fang, and Hanqing Lu. Dual attention network for scene segmentation. In *Proceedings of the IEEE Conference on Computer Vision and Pattern Recognition*, pages 3146–3154, 2019.
- [41] Ashish Vaswani, Noam Shazeer, Niki Parmar, Jakob Uszkoreit, Llion Jones, Aidan N Gomez, Lukasz Kaiser, and Illia Polosukhin. Attention is all you need. In *Advances in neural information processing systems*, pages 5998–6008, 2017.
- [42] Tsung-Yi Lin, Piotr Dollár, Ross Girshick, Kaiming He, Bharath Hariharan, and Serge Belongie. Feature pyramid networks for object detection. In *Proceedings of the IEEE conference on computer vision and pattern recognition*, pages 2117–2125, 2017.
- [43] Shuai Zheng, Sadeep Jayasumana, Bernardino Romera-Paredes, Vibhav Vineet, Zhizhong Su, Dalong Du, Chang Huang, and Philip HS Torr. Conditional random fields as recurrent neural networks. In *Proceedings of the IEEE international conference on computer vision*, pages 1529–1537, 2015.
- [44] Philipp Krähenbühl and Vladlen Koltun. Efficient inference in fully connected crfs with gaussian edge potentials. *Advances in neural information processing systems*, 24:109–117, 2011.
- [45] Ning Xu, Brian Price, Scott Cohen, Jimei Yang, and Thomas S Huang. Deep interactive object selection. In *Proceedings of the IEEE Conference on Computer Vision and Pattern Recognition*, pages 373–381, 2016.
- [46] Nanqing Dong and Eric P Xing. Few-shot semantic segmentation with prototype learning. In *BMVC*, volume 3, 2018.
- [47] Kate Rakelly, Evan Shelhamer, Trevor Darrell, Alyosha A. Efros, and Sergey Levine. Conditional networks for few-shot semantic segmentation. In *6th International Conference on Learning Representations, ICLR, Vancouver, BC, Canada, Workshop Track Proceedings*, 2018.
- [48] Ayyappa Kumar Pambala, Titir Dutta, and Soma Biswas. SML: semantic meta-learning for few-shot semantic segmentation. *CoRR*, abs/2009.06680, 2020.
- [49] Pinzhao Tian, Zhangkai Wu, Lei Qi, Lei Wang, Yinghuan Shi, and Yang Gao. Differentiable meta-learning model for few-shot semantic segmentation. In *The Thirty-Fourth AAAI Conference on Artificial Intelligence, AAAI*, pages 12087–12094. AAAI Press, 2020.
- [50] Amirreza Shaban, Shray Bansal, Zhen Liu, Irfan Essa, and Byron Boots. One-shot learning for semantic segmentation. *Proceedings of the British Machine Vision Conference (BMVC)*, pages 167.1–167.13, 2017.

- [51] Xiaolin Zhang, Yunchao Wei, Yi Yang, and Thomas S. Huang. Sg-one: Similarity guidance network for one-shot semantic segmentation. *IEEE Transactions on Cybernetics*, 50(9):3855–3865, 2020.
- [52] Kaixin Wang, Jun Hao Liew, Yingtian Zou, Daquan Zhou, and Jiashi Feng. Panet: Few-shot image semantic segmentation with prototype alignment. In *Proceedings of the IEEE/CVF International Conference on Computer Vision (ICCV)*, October 2019.
- [53] Chi Zhang, Guosheng Lin, Fayao Liu, Rui Yao, and Chunhua Shen. Canet: Class-agnostic segmentation networks with iterative refinement and attentive few-shot learning. In *Proceedings of the IEEE/CVF Conference on Computer Vision and Pattern Recognition (CVPR)*, June 2019.
- [54] Haochen Wang, Xudong Zhang, Yutao Hu, Yandan Yang, Xianbin Cao, and Xiantong Zhen. Few-shot semantic segmentation with democratic attention networks. In *Computer Vision - ECCV 2020 - 16th European Conference, Glasgow, UK, August 23-28, 2020, Proceedings, Part XIII*, volume 12358 of *Lecture Notes in Computer Science*, pages 730–746. Springer, 2020.
- [55] Chi Zhang, Guosheng Lin, Fayao Liu, Jiushuang Guo, Qingyao Wu, and Rui Yao. Pyramid graph networks with connection attentions for region-based one-shot semantic segmentation. In *Proceedings of the IEEE/CVF International Conference on Computer Vision (ICCV)*, October 2019.
- [56] Boyu Yang, Chang Liu, Bohao Li, Jianbin Jiao, and Qixiang Ye. Prototype mixture models for few-shot semantic segmentation. In *Computer Vision - ECCV 2020 - 16th European Conference, Glasgow, UK, August 23-28, 2020, Proceedings, Part VIII*, volume 12353 of *Lecture Notes in Computer Science*, pages 763–778. Springer, 2020.
- [57] Karen Simonyan and Andrew Zisserman. Very deep convolutional networks for large-scale image recognition. In *3rd International Conference on Learning Representations, ICLR 2015, San Diego, CA, USA, May 7-9, 2015, Conference Track Proceedings*, 2015.
- [58] Christian Szegedy, Wei Liu, Yangqing Jia, Pierre Sermanet, Scott Reed, Dragomir Anguelov, Dumitru Erhan, Vincent Vanhoucke, and Andrew Rabinovich. Going deeper with convolutions. In *2015 IEEE Conference on Computer Vision and Pattern Recognition (CVPR)*, pages 1–9, 2015.
- [59] François Chollet. Xception: Deep learning with depthwise separable convolutions. In *2017 IEEE Conference on Computer Vision and Pattern Recognition (CVPR)*, pages 1800–1807, 2017.
- [60] Laurent Sifre and Stéphane Mallat. Rigid-motion scattering for texture classification. *arXiv preprint arXiv:1403.1687*, 2014.
- [61] Min Lin, Qiang Chen, and Shuicheng Yan. Network in network. In *2nd International Conference on Learning Representations, ICLR 2014, Banff, AB, Canada, April 14-16, 2014, Conference Track Proceedings*, 2014.
- [62] Sergey Ioffe and Christian Szegedy. Batch normalization: Accelerating deep network training by reducing internal covariate shift. In *International conference on machine learning*, pages 448–456. PMLR, 2015.
- [63] Vinod Nair and Geoffrey E Hinton. Rectified linear units improve restricted boltzmann machines. In *Icml*, 2010.
- [64] Gao Huang, Shichen Liu, Laurens van der Maaten, and Kilian Q. Weinberger. Condensenet: An efficient densenet using learned group convolutions. In *2018 IEEE/CVF Conference on Computer Vision and Pattern Recognition*, pages 2752–2761, 2018.
- [65] Adam Paszke, Sam Gross, Francisco Massa, Adam Lerer, James Bradbury, Gregory Chanan, Trevor Killeen, Zeming Lin, Natalia Gimelshein, Luca Antiga, Alban Desmaison, Andreas Kopf, Edward Yang, Zachary DeVito, Martin Raison, Alykhan Tejani, Sasank Chilamkurthy, Benoit Steiner, Lu Fang, Junjie Bai, and Soumith Chintala. Pytorch: An imperative style, high-performance deep learning library. In *Advances in Neural Information Processing Systems 32*, pages 8024–8035. Curran Associates, Inc., 2019.

- [66] Herbert Robbins and Sutton Monro. A stochastic approximation method. *The annals of mathematical statistics*, pages 400–407, 1951.
- [67] Mark Sandler, Andrew Howard, Menglong Zhu, Andrey Zhmoginov, and Liang-Chieh Chen. Mobilenetv2: Inverted residuals and linear bottlenecks. In *2018 IEEE/CVF Conference on Computer Vision and Pattern Recognition*, pages 4510–4520, 2018.
- [68] Mingxing Tan and Quoc V. Le. Efficientnet: Rethinking model scaling for convolutional neural networks. In *Proceedings of the 36th International Conference on Machine Learning, ICML 2019, 9-15 June 2019, Long Beach, California, USA*, volume 97 of *Proceedings of Machine Learning Research*, pages 6105–6114. PMLR, 2019.
- [69] Ilija Radosavovic, Raj Prateek Kosaraju, Ross Girshick, Kaiming He, and Piotr Dollár. Designing network design spaces. In *Proceedings of the IEEE/CVF Conference on Computer Vision and Pattern Recognition*, pages 10428–10436, 2020.
- [70] Yurii E Nesterov. A method for solving the convex programming problem with convergence rate  $o(1/k^2)$ . In *Dokl. akad. nauk Sssr*, volume 269, pages 543–547, 1983.
- [71] Jia Deng, Wei Dong, Richard Socher, Li-Jia Li, Kai Li, and Li Fei-Fei. Imagenet: A large-scale hierarchical image database. In *2009 IEEE conference on computer vision and pattern recognition*, pages 248–255. Ieee, 2009.
- [72] jfzhang95. pytorch-deeplab-xception (deeplabv3+ with resnet-101 backbone). <https://github.com/jfzhang95/pytorch-deeplab-xception>.
- [73] stigma0617. Vovnet-deeplabv3 (deeplabv3 with densenet161 backbone). <https://github.com/stigma0617/VoVNet-DeepLabV3>.
- [74] Ke Sun, Yang Zhao, Borui Jiang, Tianheng Cheng, Bin Xiao, Dong Liu, Yadong Mu, Xinggang Wang, Wenyu Liu, and Jingdong Wang. Hrnet-semantic-segmentation. <https://github.com/HRNet/HRNet-Semantic-Segmentation>.
- [75] milesial. Pytorch-unet. <https://github.com/milesial/Pytorch-UNet>.
- [76] Saining Xie, Ross Girshick, Piotr Dollár, Zhuowen Tu, and Kaiming He. Aggregated residual transformations for deep neural networks. In *2017 IEEE Conference on Computer Vision and Pattern Recognition (CVPR)*, pages 5987–5995, 2017.
- [77] Pavel Yakubovskiy. Segmentation models pytorch. [https://github.com/qubvel/segmentation\\_models\\_pytorch](https://github.com/qubvel/segmentation_models_pytorch), 2020.
- [78] Marius Cordts, Mohamed Omran, Sebastian Ramos, Timo Rehfeld, Markus Enzweiler, Rodrigo Benenson, Uwe Franke, Stefan Roth, and Bernt Schiele. The cityscapes dataset for semantic urban scene understanding. In *Proceedings of the IEEE conference on computer vision and pattern recognition*, pages 3213–3223, 2016.
- [79] Ke Sun, Bin Xiao, Dong Liu, and Jingdong Wang. Deep high-resolution representation learning for human pose estimation. In *CVPR*, 2019.
- [80] Vladislav Sovrasov. flops-counter.pytorch. <https://github.com/sovrasov/flops-counter.pytorch>.
- [81] Gabriel J. Brostow, Jamie Shotton, Julien Fauqueur, and Roberto Cipolla. Segmentation and recognition using structure from motion point clouds. In *ECCV (1)*, pages 44–57, 2008.
- [82] Alex Kendall. Segnet-tutorial. <https://github.com/alexgkendall/SegNet-Tutorial>.
- [83] Hassan Alhaija, Siva Mustikovela, Lars Mescheder, Andreas Geiger, and Carsten Rother. Augmented reality meets computer vision: Efficient data generation for urban driving scenes. *International Journal of Computer Vision (IJCV)*, 2018.

## A Appendix

### A.1 Extended data ablation study

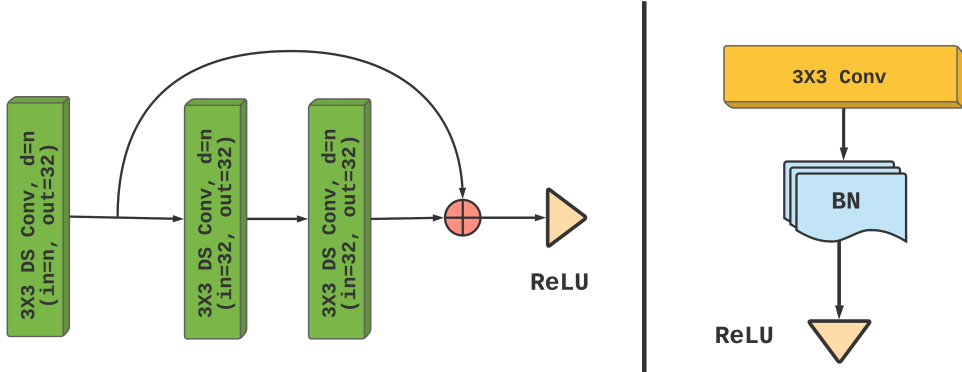


Figure 3: The glance module of PDFNet

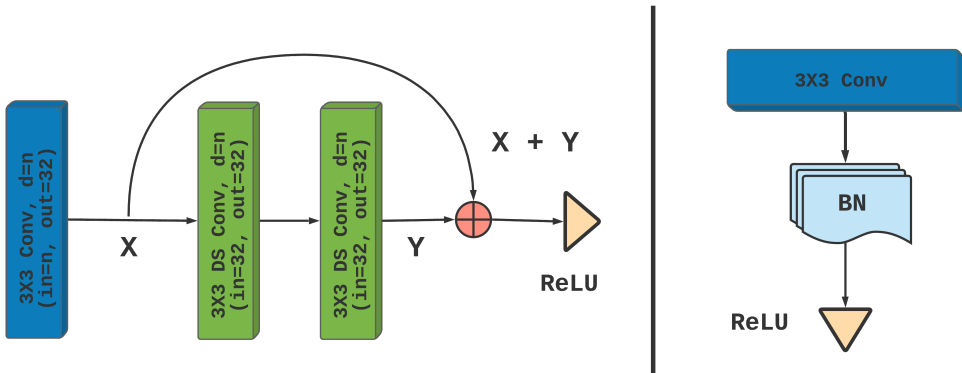


Figure 4: The glance module of DFNet

The PDFNet variants (PDFNet12 (1.2M), PDFNet9 (758K), PDFNet6 (405K), and PDFNet3 (164K)) consists of fewer parameters than any baseline network. Here, one might argue that the network size of the PDFNet variants is very less compared to any baseline network.

Hence, we conduct additional experiments to verify whether the performance gains of PDFNet on few data samples are due to the proposed architecture or not.

In Figure 3, we present the glance module of PDFNet. We modified the PDFNet-glance module by replacing the first Conv layer with a regular Conv layer, as shown in Figure 4.

We design DFNet variants (DFNet12 (7.6M), DFNet9 (4.6M), DFNet6 (2.3M), and DFNet3 (0.9M)) by replacing the original glance module with modified glance module in PDFNet variants.

We train each network on five different subsets of training data  $T_{1487}$ ,  $T_{743}$ ,  $T_{371}$ ,  $T_{185}$ , and  $T_{92}$  and provide the results in Table 5 (including results from the main paper).

From Table 5, we observe that:

- (i) The DFNet variants outperformed all the baseline networks.
  - (ii) The PDFNet variants outperforms DFNet variants while requiring fewer parameters and GFLOPs.
- From the above, we verify that the performance gains of PDFNet on few data samples are due to the proposed architecture and not due to the less size of the network.

Moreover, we provide the class-wise IoU results of the data ablation experiments in Table 6.

Backbone	$T_{1487}$	$T_{743}$	$T_{371}$	$T_{185}$	$T_{92}$	$T_{avg}$	Param(M)	GFLOPS
ResNet-18	42.6	35.6	27.9	22.4	21.0	29.9	12.3	36.8
MobileNet-V2	38.5	32.2	30.6	22.5	19.2	28.6	4.4	12.3
EfficientNet-b1	37.8	32.5	26.9	24.6	19.8	28.3	7.4	4.6
RegNetY-08	28.5	31.9	29.4	27.4	22.1	27.9	7.0	17.2
ResNet-101	29.3	28.8	28.6	21.6	19.4	25.5	59.3	177.8
DenseNet-161	33.3	30.1	26.0	24.9	20.8	27.0	43.2	129.4
HRNet-V2	27.8	18.8	23.3	18.3	15.4	20.7	65.9	187.8
U-Net	42.8	34.2	30.2	27.8	25.0	32.0	31.0	387.1
PDFNet3	47.1	42.9	39.9	34.7	29.7	38.9	0.2	8.0
PDFNet6	49.6	43.2	39.1	<b>35.8</b>	<b>30.5</b>	39.6	0.4	10.3
PDFNet9	48.8	44.9	<b>40.0</b>	34.1	29.3	39.4	0.8	13.5
PDFNet12	50.8	<b>46.6</b>	38.5	33.8	30.3	<b>40.0</b>	1.2	17.5
PDFNet3-2S	44.7	40.0	34.0	33.4	29.9	36.4	<b>0.1</b>	<b>2.7</b>
PDFNet6-2S	46.9	40.5	38.2	32.6	24.3	36.5	0.3	4.5
PDFNet9-2S	47.3	43.7	35.9	32.9	27.6	37.5	0.7	7.5
PDFNet12-2S	46.0	40.1	36.9	31.4	28.0	36.5	1.1	11.1
DFNet3	48.8	44.4	35.9	32.5	28.5	38.0	0.9	28.1
DFNet6	50.9	<b>46.6</b>	37.1	34.0	28.6	39.4	2.3	42.1
DFNet9	<b>52.2</b>	43.0	36.9	34.1	28.7	39.0	4.6	61.7
DFNet12	49.4	44.4	38.2	33.5	29.2	38.9	7.6	86.9

Table 5: Cityscapes additional data ablation experiments evaluated on the validation set

### A.1.1 Training plots

For ease of visualization, we divide the Cityscapes experiments training plots into three sets.

Set-1 consists of ResNet-101, DenseNet-161, HRNet-V2, U-Net, and PDFNet12 (shown in Figure 5).

Set-2 consists of ResNet-18, MobileNet-V2, EfficientNet-b1, RegNetY-08, and PDFNet12 (shown in Figure 6).

Set-3 consists of PDFNet3, PDFNet6, PDFNet9, and PDFNet12 (shown in Figure 7).

### A.2 Qualitative results

In Figure 8, we present the qualitative results of the networks HRNet-V2 (48.0), U-Net (49.3), and PDFNet12 (54.9) from the Cityscapes baseline experiments.



Subset	Method	road	sidewalk	building	wall	fence	pole	traffic light	traffic sign	vegetation	terrain	sky	person	rider	car	truck	bus	train	motorcycle	bicycle	Average
T <sub>1487</sub>	ResNet18	93.7	64.4	81.5	14.5	13.8	27.8	17.8	26.3	85.0	46.2	88.8	46.7	7.4	81.3	23.8	34.5	10.1	5.0	39.6	42.6
	MobileNetV2	93.9	64.6	81.8	15.8	16.2	24.0	1.0	17.6	84.4	39.9	88.6	39.2	0.0	82.5	13.0	26.8	9.0	0.0	32.6	38.5
	EfficientNetB1	93.3	64.9	81.7	0.3	15.0	26.2	2.5	23.8	83.7	41.4	88.6	42.3	0.0	81.9	0.0	25.7	17.0	0.0	30.7	37.8
	RegNetY08	94.1	57.7	77.6	0.0	0.3	0.0	0.0	0.0	82.0	41.4	88.4	25.7	0.0	75.0	0.0	0.0	0.0	0.0	0.0	28.5
	ResNet101-1	93.0	54.0	75.9	12.9	0.9	3.4	0.0	0.2	81.7	38.8	86.9	30.9	0.0	73.7	2.7	0.0	0.0	0.0	1.0	29.3
	DenseNet161-1	93.1	57.7	78.9	11.2	6.6	11.1	0.0	12.4	81.5	38.3	84.9	35.0	0.0	76.7	13.4	0.3	2.3	0.1	28.3	33.3
	HRNet-V2	92.3	52.3	76.9	0.7	0.5	0.0	0.0	0.0	81.8	34.5	82.9	9.4	0.0	72.3	0.0	5.3	0.0	0.0	18.6	27.8
	U-Net	94.0	65.6	83.2	13.9	20.5	34.3	21.7	43.9	87.4	43.1	89.5	49.9	0.0	84.2	12.1	9.9	12.9	0.0	47.9	42.8
	PDFNet3	93.9	68.2	84.7	25.2	<b>33.6</b>	39.2	25.4	44.6	87.1	48.7	<b>90.4</b>	49.6	6.1	84.5	15.2	31.8	13.1	5.3	48.6	47.1
	PDFNet6	93.6	69.6	84.7	25.9	32.1	40.1	29.2	47.2	87.1	49.2	90.3	54.2	<b>18.2</b>	84.8	20.5	37.6	18.6	5.9	<b>53.0</b>	49.6
	PDFNet9	93.7	70.5	<b>85.1</b>	23.2	31.8	39.4	<b>30.2</b>	44.9	87.1	47.3	90.3	52.6	14.1	85.4	16.0	39.2	<b>23.5</b>	2.8	50.2	48.8
	PDFNet12	<b>95.2</b>	<b>71.0</b>	84.9	31.9	32.2	<b>41.6</b>	28.9	<b>47.8</b>	<b>87.6</b>	<b>51.4</b>	90.2	<b>55.4</b>	15.1	<b>85.9</b>	<b>26.0</b>	<b>43.1</b>	18.1	<b>8.4</b>	50.2	<b>50.8</b>
	PDFNet3-2S	94.5	67.0	83.3	15.8	25.5	35.0	22.7	39.7	86.1	44.2	89.7	48.2	4.9	82.6	15.0	35.4	8.3	6.4	46.0	44.7
	PDFNet6-2S	93.5	68.3	83.2	20.7	33.0	38.0	24.5	40.4	85.8	48.1	88.6	51.1	10.9	83.5	19.7	29.2	19.3	5.7	47.7	46.9
PDFNet9-2S	94.2	68.4	83.9	<b>33.3</b>	30.8	37.8	16.9	38.8	86.5	48.6	89.8	49.9	6.8	84.1	20.8	31.7	19.9	7.4	48.6	47.3	
PDFNet12-2s	94.2	66.0	84.0	21.6	27.9	32.9	21.1	40.7	86.5	49.1	89.1	48.6	4.6	83.8	18.9	38.9	16.1	4.9	44.1	46.0	
T <sub>743</sub>	ResNet18	92.8	56.3	78.0	15.3	8.0	15.4	4.9	18.9	82.3	42.8	85.6	35.4	0.1	75.2	13.1	13.9	1.9	0.0	36.6	35.6
	MobileNetV2	92.7	57.3	77.8	6.1	7.8	0.7	0.1	11.3	81.5	39.2	85.2	30.8	0.1	75.9	3.5	22.9	2.9	0.0	15.4	32.2
	EfficientNetB1	93.5	60.5	77.1	4.1	3.9	9.1	0.0	14.0	81.8	39.6	84.6	22.8	1.6	75.1	9.8	18.6	0.0	0.0	20.8	32.5
	RegNetY08	93.9	58.7	78.8	3.4	9.1	0.0	0.0	17.5	83.1	45.2	87.1	32.0	0.0	76.8	2.3	0.3	0.0	0.0	17.1	31.9
	ResNet101	90.5	44.6	72.2	9.2	3.3	5.2	0.0	12.5	79.8	36.2	79.8	25.6	0.0	65.3	0.0	0.0	0.0	0.0	0.0	28.8
	DenseNet161	91.1	50.8	74.7	13.9	3.3	4.4	1.1	12.1	78.4	32.1	80.8	28.6	0.0	69.6	2.2	1.4	0.2	2.3	25.7	30.1
	HRNet-V2	86.0	23.6	62.0	0.0	0.0	0.0	0.0	0.0	60.3	10.9	78.1	0.0	0.0	37.3	0.0	0.0	0.0	0.0	0.0	18.8
	U-Net	93.9	62.1	81.3	5.2	11.6	19.3	0.4	28.1	86.0	42.5	87.8	36.5	0.5	79.6	9.6	0.0	0.0	0.0	5.5	34.2
	PDFNet3	<b>93.8</b>	63.7	81.6	17.6	21.1	30.5	12.3	31.3	84.2	42.4	88.2	43.6	1.0	79.4	10.4	19.3	3.4	1.0	36.1	40.0
	PDFNet6	<b>94.0</b>	65.1	83.2	17.2	25.9	34.9	17.5	38.9	85.9	44.2	90.0	46.6	1.2	81.2	17.1	24.9	9.6	0.3	43.7	43.2
	PDFNet9	93.9	66.9	83.4	19.5	25.3	36.3	23.8	40.4	85.6	43.9	88.9	48.7	2.1	82.8	17.1	34.6	<b>10.3</b>	2.4	47.5	44.9
	PDFNet12	93.4	<b>68.9</b>	<b>84.1</b>	<b>30.0</b>	<b>33.0</b>	<b>38.3</b>	<b>26.0</b>	<b>46.9</b>	<b>86.5</b>	<b>49.5</b>	<b>89.2</b>	<b>50.2</b>	<b>14.2</b>	<b>83.9</b>	15.4	<b>27.5</b>	2.8	1.7	<b>47.8</b>	<b>46.6</b>
	PDFNet3-2S	90.2	49.5	74.4	5.6	10.9	15.3	0.0	8.2	79.0	34.6	82.1	22.6	0.0	68.6	1.1	0.9	4.2	0.0	17.5	29.7
	PDFNet6-2S	93.5	63.4	81.7	18.6	17.2	31.2	13.5	30.0	85.0	42.5	88.2	42.6	0.9	80.5	8.0	27.2	4.6	1.5	39.5	40.5
PDFNet9-2S	94.0	65.9	82.6	27.7	22.4	34.8	18.0	35.4	85.5	45.1	88.9	47.2	7.7	82.8	<b>18.6</b>	23.4	3.2	<b>4.4</b>	43.3	43.7	
PDFNet12-2s	93.5	62.0	81.7	14.1	22.3	32.8	12.7	29.8	83.9	38.9	87.5	43.3	1.9	80.4	8.9	21.6	6.4	0.5	39.0	40.1	
T <sub>371</sub>	ResNet18	88.4	46.5	73.5	2.6	1.1	4.0	0.0	5.3	78.4	36.4	82.9	27.9	0.0	68.5	0.0	0.0	0.0	1.4	13.1	27.9
	MobileNetV2	91.4	50.2	75.2	10.1	7.3	5.6	0.3	8.5	81.0	34.6	83.0	27.8	0.0	72.7	<b>16.0</b>	1.4	0.0	0.0	16.6	30.6
	EfficientNetB1	89.8	46.4	72.4	5.3	4.9	7.6	0.3	6.5	75.7	32.7	77.3	20.7	0.0	65.1	0.0	0.0	0.0	0.0	6.8	26.9
	RegNetY08	91.6	50.5	76.3	10.3	5.8	0.0	0.3	10.3	81.2	38.3	84.5	26.2	0.0	70.6	8.1	0.0	0.0	0.0	3.8	29.4
	ResNet101	89.2	45.8	73.6	9.8	2.7	3.1	0.0	8.0	79.9	34.8	81.6	26.9	0.0	65.3	8.9	0.0	0.0	0.0	13.8	28.6
	DenseNet161	89.0	42.4	71.9	8.1	2.1	0.0	0.0	0.0	75.7	33.8	77.4	18.6	0.0	64.3	3.3	0.2	0.0	0.0	6.2	26.0
	HRNet-V2	87.4	35.3	68.7	0.1	0.0	0.0	0.0	0.0	71.7	33.9	76.4	8.9	0.0	56.2	0.0	0.0	0.0	0.0	0.3	23.3
	U-Net	92.3	57.4	76.9	4.7	7.4	2.7	1.2	14.1	83.4	36.6	85.8	28.5	0.0	75.8	3.3	0.0	1.9	0.0	1.4	30.2
	PDFNet3	92.5	54.0	78.1	9.5	15.8	21.1	0.0	17.0	<b>82.0</b>	38.2	86.3	36.6	0.0	74.9	0.8	8.3	2.7	0.0	28.5	34.0
	PDFNet6	93.2	<b>61.2</b>	80.7	11.9	17.9	28.4	3.7	26.9	<b>84.6</b>	<b>40.8</b>	87.4	39.7	0.0	78.5	15.6	<b>30.3</b>	6.9	0.2	35.7	39.1
	PDFNet9	93.3	<b>61.2</b>	<b>81.0</b>	15.1	<b>19.3</b>	<b>29.3</b>	8.0	30.0	83.9	39.8	87.8	41.3	<b>6.3</b>	<b>79.0</b>	11.5	26.3	<b>8.9</b>	<b>0.3</b>	<b>37.0</b>	<b>40.0</b>
	PDFNet12	92.6	61.1	<b>81.0</b>	<b>24.8</b>	14.9	<b>30.2</b>	<b>9.5</b>	<b>33.2</b>	84.0	36.2	<b>88.0</b>	<b>42.0</b>	0.5	78.7	14.1	6.7	0.0	<b>3.3</b>	30.6	38.5
	PDFNet3-2S	90.2	49.5	74.4	5.6	10.9	15.3	0.0	8.2	79.0	34.6	82.1	22.6	0.0	68.6	1.1	0.9	4.2	0.0	17.5	29.7
	PDFNet6-2S	92.8	60.4	79.6	8.7	17.2	27.6	5.5	29.2	83.0	40.4	87.4	39.9	0.4	77.9	8.5	24.2	7.4	0.1	36.1	38.2
PDFNet9-2S	92.6	60.3	79.1	18.0	13.7	24.8	4.8	16.1	82.8	38.2	87.3	36.2	0.0	76.5	12.2	10.6	0.0	0.0	29.0	35.9	
PDFNet12-2s	<b>93.5</b>	58.2	79.0	13.3	14.6	28.6	5.4	25.4	82.5	39.7	86.1	38.8	1.3	77.8	2.8	17.7	3.7	0.0	31.8	36.9	
T <sub>185</sub>	ResNet18	85.0	32.3	70.4	1.6	0.0	0.0	0.0	0.0	75.9	32.0	80.0	0.0	0.0	53.0	0.0	0.0	0.0	0.0	0.0	22.4
	MobileNetV2	85.9	37.3	68.8	0.0	0.0	0.0	0.0	0.0	74.1	34.6	71.3	0.0	0.0	54.6	0.0	0.0	0.0	0.0	0.0	22.5
	EfficientNetB1	85.2	38.8	71.0	4.1	1.5	0.0	0.0	0.2	78.6	31.8	80.0	17.9	0.0	58.1	0.0	0.0	0.0	0.0	0.0	24.6
	RegNetY08	89.4	47.2	74.3	6.5	2.5	0.0	0.2	8.2	78.9	35.7	82.6	22.4	0.0	66.9	3.1	0.0	0.0	0.0	2.2	27.4
	ResNet101	85.4	29.7	66.9	0.0	0.0	0.0	0.0	0.0	73.4	31.3	75.0	0.0	0.0	48.5	0.0	0.0	0.0	0.0	0.0	21.6
	DenseNet161	87.8	40.2	72.2	3.2	2.4	0.0	0.0	0.0	76.9	28.3	78.6	15.2	0.0	61.5	2.3	0.0	0.0	0.0	5.1	24.9
	HRNet-V2	86.4	19.3	63.8	0.0	0.0	0.0	0.0	0.0	67.9	0.0	70.6	0.0	0.0	38.8	0.0	0.0	0.0	0.0	0.0	18.3
	U-Net	90.2	50.1	74.0	7.5	0.6	0.0	0.0	8.1	81.1	33.1	82.7	13.2	0.0	68.4	0.0	0.0	0.6	0.2	18.4	27.8
	PDFNet3	<b>92.1&lt;/</b>																			

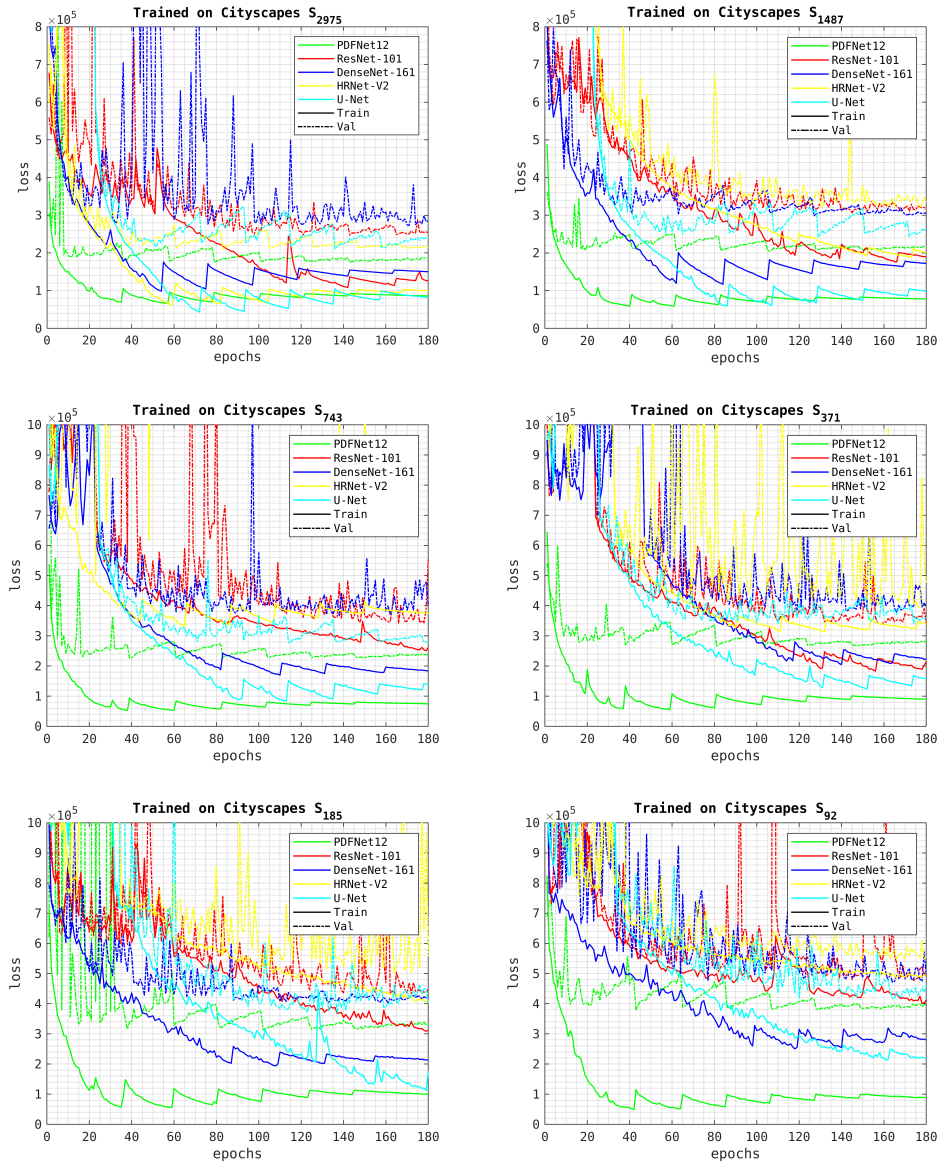


Figure 5: Cityscapes Set-1 training plots

## B CamVid

In Figure 9, we present the training plots of the networks ResNet-18, EfficientNet-b1, RegNetY-08, MobileNet-V2, PDFNet3, and PDFNet6, trained on three subsets of training data ( $T_{367}$ ,  $T_{183}$ , and  $T_{91}$ ).

In Figure 10, we present the training plots of the networks ResNet-50, EfficientNet-b4, RegNetY-40, ResNext-50, and PDFNet9, trained on three subsets of training data ( $T_{367}$ ,  $T_{183}$ , and  $T_{91}$ ).

In Figure 11, we present the training plots of the networks ResNet-101, EfficientNet-b6, RegNetY-80, DenseNet-161, HRNet-V2, U-Net, and PDFNet12, trained on three subsets of training data ( $T_{367}$ ,  $T_{183}$ , and  $T_{91}$ ).

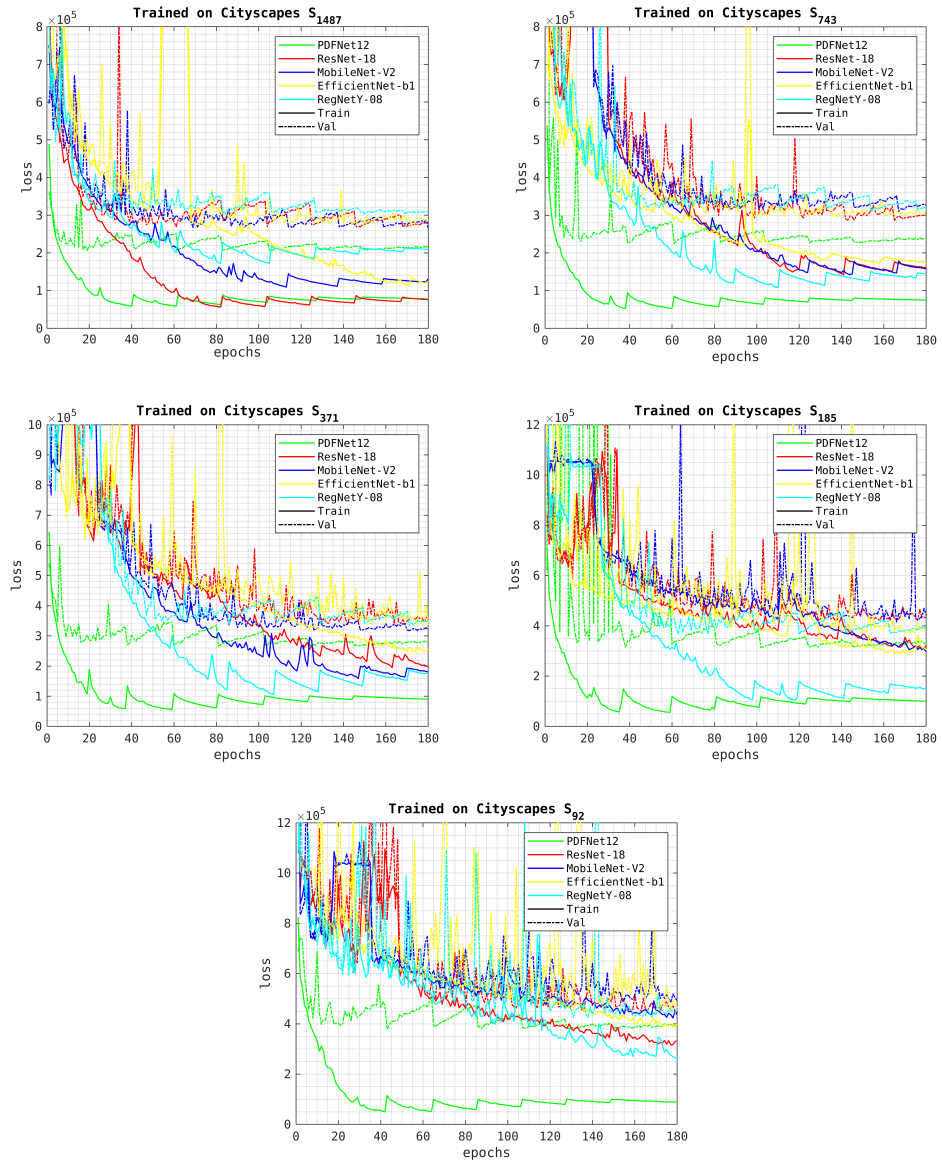


Figure 6: Cityscapes Set-2 training plots

## C KITTI

In Table 7, we provide the class-wise results of the data ablation experiments evaluated on the KITTI training set.

Subset	Method	road	sidewalk	building	wall	fence	pole	traffic light	traffic sign	vegetation	terrain	sky	person	rider	car	truck	bus	train	motorcycle	bicycle	Average
T <sub>1487</sub>	ResNet18	55.2	13.4	25.0	1.0	4.8	8.8	15.5	8.8	59.5	10.1	40.0	2.4	<b>0.6</b>	26.1	1.5	4.9	8.7	0.0	0.6	15.1
	MobileNetV2	61.0	11.2	44.4	3.9	8.7	19.0	2.1	<b>10.3</b>	73.2	17.2	<b>56.2</b>	2.0	0.0	<b>52.5</b>	3.2	<b>33.4</b>	11.9	0.0	0.4	<b>21.6</b>
	EfficientNetB1	62.9	<b>18.5</b>	40.3	0.0	9.8	16.3	13.2	7.9	<b>74.3</b>	21.5	54.9	1.7	0.3	47.5	0.0	0.7	0.0	0.0	1.1	19.5
	RegNetY08	47.0	5.2	26.1	0.0	0.2	0.0	0.0	0.0	52.9	6.1	45.0	0.5	0.0	22.8	0.0	0.0	0.0	0.0	0.0	10.8
	ResNet101	46.7	7.1	32.0	0.3	5.1	8.6	1.6	2.3	43.7	8.4	39.1	0.8	0.0	28.0	1.6	0.1	1.7	0.0	0.2	12.9
	DenseNet161	49.5	2.0	19.9	0.5	1.4	3.1	0.2	5.2	47.1	9.7	36.5	0.9	0.0	26.8	0.6	0.0	5.4	0.0	0.2	10.5
	HRNet-V2	48.9	5.6	13.7	0.6	0.3	0.0	0.0	0.0	28.6	6.3	7.7	0.2	0.0	20.0	0.0	0.0	0.0	0.0	0.1	6.9
	UNet	50.6	2.5	33.4	4.5	5.6	7.9	11.0	4.2	57.3	4.9	43.5	1.3	0.0	32.7	1.6	1.7	3.9	0.0	0.4	14.1
	PDFNet3	61.5	3.9	35.0	<b>11.8</b>	13.4	17.0	12.7	6.1	69.5	8.4	47.9	0.9	0.0	30.2	1.8	0.2	4.1	0.0	2.0	17.2
	PDFNet6	54.5	5.4	<b>46.5</b>	10.5	14.9	21.1	<b>18.3</b>	5.1	74.1	10.7	52.0	1.6	0.0	33.4	3.7	7.6	5.2	0.0	0.8	19.2
	PDFNet9	61.2	4.5	41.9	3.9	<b>20.3</b>	<b>24.4</b>	14.0	8.0	73.9	17.4	45.3	1.9	0.2	37.0	<b>4.1</b>	<b>16.7</b>	<b>20.2</b>	0.0	1.4	20.9
	PDFNet12	60.6	5.4	33.2	7.4	12.2	19.7	17.3	9.7	69.8	23.3	47.3	1.2	0.2	29.9	1.6	2.4	3.4	0.0	<b>3.0</b>	18.3
	PDFNet3-2S	46.3	7.3	34.4	6.6	6.2	15.6	7.3	5.6	53.0	10.6	40.9	0.8	0.4	29.2	0.4	4.8	0.6	0.0	1.2	14.3
	PDFNet6-2S	63.4	13.0	35.2	11.3	13.5	20.7	11.0	6.3	58.5	10.6	44.4	1.1	0.2	46.1	1.5	10.7	16.7	0.0	2.6	19.4
PDFNet9-2S	53.4	15.0	38.5	0.4	2.7	10.6	0.1	2.8	66.9	7.4	44.1	1.1	0.0	27.9	0.1	1.8	3.0	0.0	0.9	14.6	
PDFNet12-2s	<b>66.1</b>	6.2	40.5	11.5	12.2	17.0	4.5	5.3	69.0	<b>26.7</b>	51.5	<b>2.7</b>	0.0	24.6	1.3	3.2	9.4	0.0	2.4	18.6	
T <sub>743</sub>	ResNet18	54.7	11.7	23.8	2.6	2.7	6.6	7.3	2.9	45.1	3.1	38.5	0.6	0.0	24.7	1.2	0.0	2.8	0.0	0.3	12.0
	MobileNetV2	61.1	13.1	38.0	2.8	5.3	2.7	0.2	3.7	60.7	11.9	<b>62.3</b>	1.3	0.0	<b>43.9</b>	1.5	0.5	6.1	0.0	0.1	17.2
	EfficientNetB1	55.6	10.5	33.9	0.0	1.4	2.4	0.0	4.0	69.3	13.7	61.7	0.8	<b>0.4</b>	34.5	0.7	0.1	0.0	0.0	0.3	15.5
	RegNetY08	55.6	9.6	31.0	0.1	3.5	0.0	0.1	3.9	54.2	10.9	46.2	1.0	0.0	26.4	1.9	0.0	0.0	0.0	0.5	12.9
	ResNet101	45.8	0.3	29.5	0.0	1.2	4.8	0.0	1.6	59.1	14.4	38.3	0.5	0.0	24.8	0.0	0.0	0.0	0.0	0.5	11.6
	DenseNet161	48.6	5.1	17.3	2.1	0.2	1.7	0.1	3.0	22.1	2.3	28.5	0.5	0.0	20.0	0.4	0.0	0.0	0.0	0.3	8.0
	HRNet-V2	41.1	6.0	16.8	0.0	0.0	0.0	0.0	0.0	36.6	9.8	23.6	0.0	0.0	19.2	0.0	0.0	0.0	0.0	0.0	8.1
	UNet	38.7	1.0	38.3	0.1	3.9	7.8	1.1	2.8	56.9	12.7	48.8	0.8	0.0	27.1	1.5	0.9	0.0	0.0	0.1	12.8
	PDFNet3	47.7	5.8	33.8	7.2	6.8	9.6	3.4	<b>7.3</b>	49.1	7.3	44.1	0.7	0.0	20.0	1.0	1.7	1.1	0.0	0.1	13.0
	PDFNet6	54.5	5.4	<b>46.5</b>	<b>10.5</b>	14.9	<b>21.1</b>	<b>18.3</b>	5.1	<b>74.1</b>	10.7	52.0	<b>1.6</b>	0.0	33.4	<b>3.7</b>	<b>7.6</b>	5.2	0.0	0.8	<b>19.2</b>
	PDFNet9	63.1	7.3	35.5	3.7	14.0	20.9	17.3	5.3	65.6	10.5	42.5	0.9	0.1	31.1	1.7	3.3	4.6	0.0	0.7	17.3
	PDFNet12	<b>68.0</b>	<b>12.5</b>	32.3	1.4	8.8	15.8	8.1	7.2	70.3	<b>17.6</b>	37.7	0.8	0.0	33.1	0.3	9.7	0.0	0.0	<b>2.1</b>	17.1
	PDFNet3-2S	47.0	5.6	31.6	4.8	4.8	9.6	5.8	3.0	53.8	3.1	43.3	0.6	0.1	14.3	0.5	1.0	1.8	0.0	0.2	12.1
	PDFNet6-2S	61.1	5.5	34.6	5.0	10.9	12.5	3.6	4.6	59.8	12.6	44.8	0.9	0.1	22.3	1.2	0.6	1.5	0.0	0.0	14.8
PDFNet9-2S	62.0	4.4	38.2	9.7	9.2	14.2	12.3	5.8	67.1	4.8	33.8	1.8	0.0	35.0	0.8	3.3	<b>14.1</b>	<b>0.1</b>	0.3	16.7	
PDFNet12-2s	55.2	8.8	37.2	5.8	<b>15.0</b>	11.8	12.4	6.5	64.2	3.1	45.7	0.8	0.1	29.5	2.3	6.1	3.8	0.0	<b>2.1</b>	16.3	
T <sub>371</sub>	ResNet18	48.8	1.4	22.0	0.0	0.3	2.4	0.0	1.9	43.5	16.7	33.4	0.7	0.0	27.4	0.0	0.0	0.0	0.0	0.1	10.5
	MobileNetV2	57.8	5.6	34.5	0.0	7.7	5.0	1.3	2.9	55.8	10.7	<b>76.8</b>	0.6	0.0	38.4	2.1	0.3	0.0	0.0	0.1	15.8
	EfficientNetB1	50.5	8.2	31.5	0.6	5.3	3.1	3.9	2.7	54.6	5.1	74.6	0.9	0.0	28.8	0.0	0.0	0.0	0.0	0.3	14.2
	RegNetY08	51.8	0.7	32.5	0.0	1.9	0.1	1.8	3.2	57.3	19.9	42.5	0.8	0.0	26.4	1.0	0.0	0.0	0.0	0.1	12.6
	ResNet101	33.1	3.7	21.9	0.0	0.5	1.6	0.0	0.0	3.8	37.8	3.8	34.1	0.5	0.0	26.0	0.7	0.0	0.0	0.0	8.8
	DenseNet161	52.1	6.5	22.1	0.3	1.0	0.0	0.0	0.0	49.5	9.6	19.9	0.3	0.0	23.7	0.0	0.0	0.0	0.0	0.1	9.7
	HRNet-V2	47.4	1.1	18.0	0.0	0.0	0.0	0.0	0.0	29.8	5.7	34.3	0.6	0.0	13.7	0.0	0.0	0.0	0.0	0.0	7.9
	UNet	36.6	0.1	20.2	0.0	0.6	2.2	0.3	2.4	51.3	1.9	39.8	0.4	0.0	19.2	0.8	0.0	0.3	0.0	0.0	9.3
	PDFNet3	55.5	6.7	<b>33.7</b>	2.2	<b>14.5</b>	14.0	7.9	<b>8.6</b>	64.1	11.0	44.2	1.3	0.1	27.7	1.9	5.8	<b>3.2</b>	0.0	0.8	16.0
	PDFNet6	50.8	8.4	<b>40.8</b>	0.4	8.3	11.4	4.5	5.6	63.2	7.0	47.5	0.7	0.0	27.6	1.3	1.9	2.8	0.0	0.3	15.2
	PDFNet9	59.1	9.8	34.2	7.3	11.5	10.8	3.8	6.4	64.2	6.0	39.3	0.8	0.3	32.3	0.2	3.0	1.9	0.3	<b>2.2</b>	15.4
	PDFNet12	<b>65.9</b>	9.2	37.2	<b>6.6</b>	9.0	10.8	<b>13.5</b>	5.7	<b>65.2</b>	<b>20.4</b>	46.0	0.7	<b>0.3</b>	<b>40.1</b>	<b>2.8</b>	3.5	0.0	<b>0.2</b>	<b>0.5</b>	<b>17.8</b>
	PDFNet3-2S	59.8	2.5	37.7	1.6	8.3	7.0	0.0	2.7	55.2	6.8	44.9	0.7	0.1	19.0	0.1	3.5	2.7	0.0	0.1	13.3
	PDFNet6-2S	48.6	<b>12.1</b>	36.7	0.8	6.4	8.2	3.6	4.1	64.7	3.4	44.6	<b>1.6</b>	0.1	28.3	0.8	<b>10.3</b>	1.4	0.0	0.6	14.5
PDFNet9-2S	59.1	9.8	34.2	7.3	11.5	10.8	3.8	6.4	64.2	6.0	39.3	0.8	<b>0.3</b>	32.3	0.2	3.0	1.9	<b>0.3</b>	<b>2.2</b>	15.4	
PDFNet12-2s	63.1	7.8	41.6	4.8	8.0	<b>16.2</b>	9.4	5.2	63.9	8.9	55.1	<b>1.6</b>	0.0	25.8	0.5	7.0	1.4	0.1	0.6	16.9	
T <sub>185</sub>	ResNet18	44.5	1.1	19.8	0.0	0.0	0.0	0.0	0.0	47.1	3.3	17.0	0.0	0.0	17.2	0.0	0.0	0.0	0.0	0.0	7.9
	MobileNetV2	57.1	12.3	28.6	0.0	0.0	0.0	0.0	0.0	55.3	<b>19.0</b>	44.0	0.0	0.0	<b>33.7</b>	0.0	0.0	0.0	0.0	0.0	13.2
	EfficientNetB1	38.9	3.5	20.3	0.0	0.2	0.0	0.0	0.1	28.8	0.9	39.2	0.4	0.0	28.1	0.0	0.0	0.0	0.0	0.0	8.1
	RegNetY08	54.9	5.5	30.8	0.0	1.3	0.0	0.8	1.4	40.6	12.0	43.0	0.5	0.0	27.1	0.2	0.0	0.0	0.0	0.0	11.5
	ResNet101	51.2	0.8	18.6	0.0	0.0	0.0	0.0	0.0	40.0	14.0	22.9	0.0	0.0	20.4	0.0	0.0	0.0	0.0	0.0	8.8
	DenseNet161	53.6	5.5	24.3	<b>2.8</b>	1.9	0.0	0.0	0.0	46.7	12.9	35.8	0.2	0.0	27.8	0.3	0.0	0.0	0.0	0.1	11.2
	HRNet-V2	54.8	5.2	25.3	0.0	0.0	0.0	0.0	0.0	42.9	0.0	32.3	0.0	0.0	17.2	0.0	0.0	0.0	0.0	0.0	9.3
	UNet	22.3	1.6	29.8	0.2	0.2	0.0	0.0	3.2	49.9	4.0	42.9	0.5	0.0	15.4	0.0	0.0	0.6	0.0	0.1	9.0
	PDFNet3	53.1	4.6	24.9	0.8	2.9	7.0	6.3	4.1	58.5	3.3	43.3	0.5	<b>0.3</b>	18.7	0.3	4.0	0.0	0.0	0.0	12.3
	PDFNet6	49.6	<b>19.4</b>	29.1	0.0	3.4	12.2	5.8	3.7	59.8	4.4	46.7	0.8	0.1	29.9	1.2	<b>6.8</b>	0.1	0.0	0.3	14.4
	PDFNet9	58.3	15.6	31.9	0.0	2.3	12.1	2.1	5.3	58.0	7.1	46.6	0.8	0.1	27.5	1.4	2.5	1.7	0.0	0.2	14.4
	PDFNet12	59.6	8.1	<b>40.3</b>	0.6	<b>5.6</b>	<b>15.3</b>	<b>13.5</b>	<b>6.0</b>	<b>67.0</b>	3.8	53.4	1.0	0.0	27.3	0.8	0.4	0.0	0.0	<b>0.6</b>	<b>16.0</b>
	PDFNet3-2S	54.9	5.2	27.5	0.3	3.4	9.8	2.8	3.8	57.1	6.3	44.6	0.6	0.0	18.3	1.6	4.5	1.4	0.0	0.1	12.7
	PDFNet6-2S	58.8	14.4	25.4	0.1	4.2	10.9	0.3	3.2	53.4	3.3	<b>46.9</b>	0.8	0.0	29.2	2.2	6.4	<b>2.8</b>	0.0	0.2	13.9
PDFNet9-2S	59.4	6.0	30.9	0.6	3.1	12.3	6.1	3.2	60.6	2.5	46.1	<b>1.2</b>	0.1	32.7	1.1	8.8	0.0	0.0	<b>0.6</b>	14.5	
PDFNet12-2s	<b>63.6</b>	9.0	30.7	1.9	1.4	11.9	0.1	4.4	66.4	6.8	44.7	1.0	0.0	30.0	1.7	0.3	<b>2.2</b>	<b>0.1</b>	<b>0.4</b>	14.6	
T <sub>92</sub>	ResNet18	52.8	4.4	22.4	0.0	0.0	0.0	0.0	0.0</												

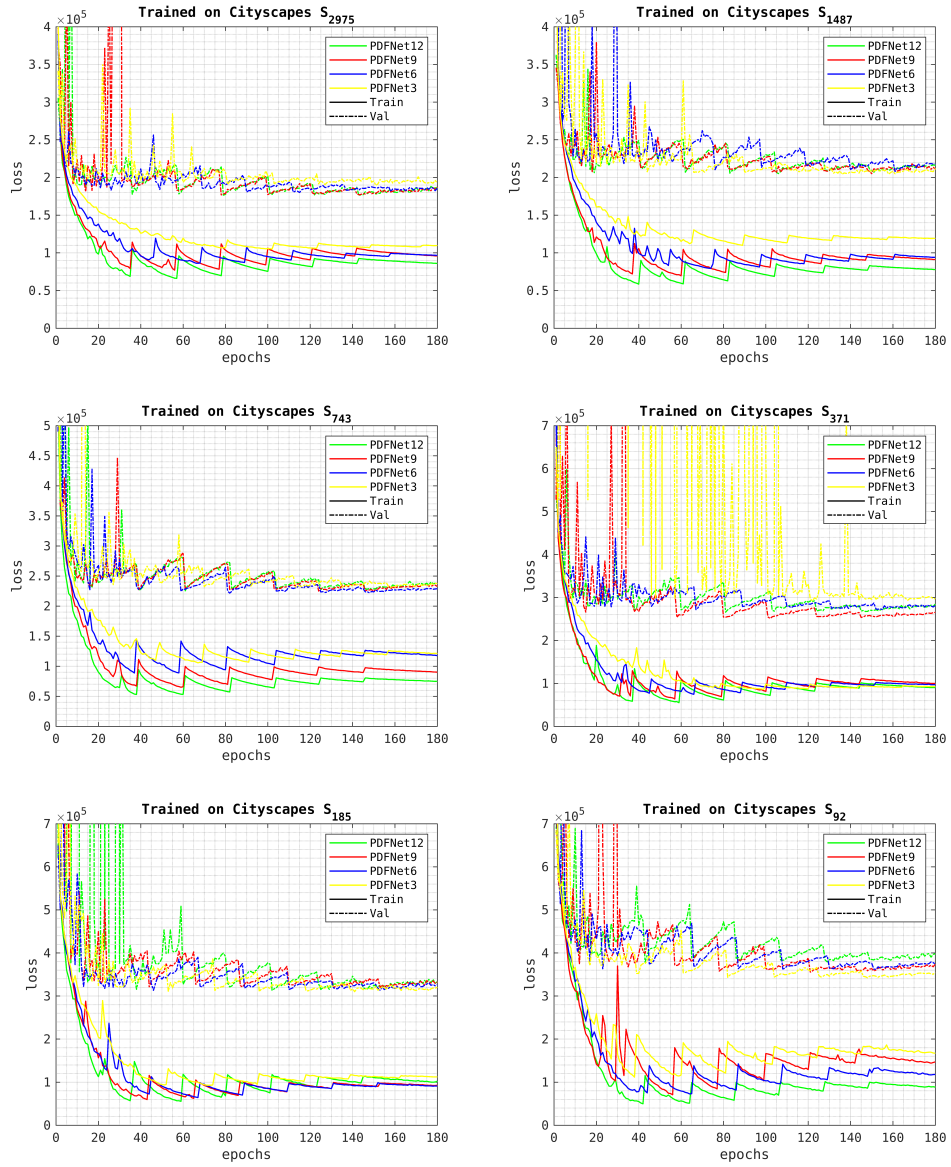


Figure 7: Cityscapes Set-3 training plots

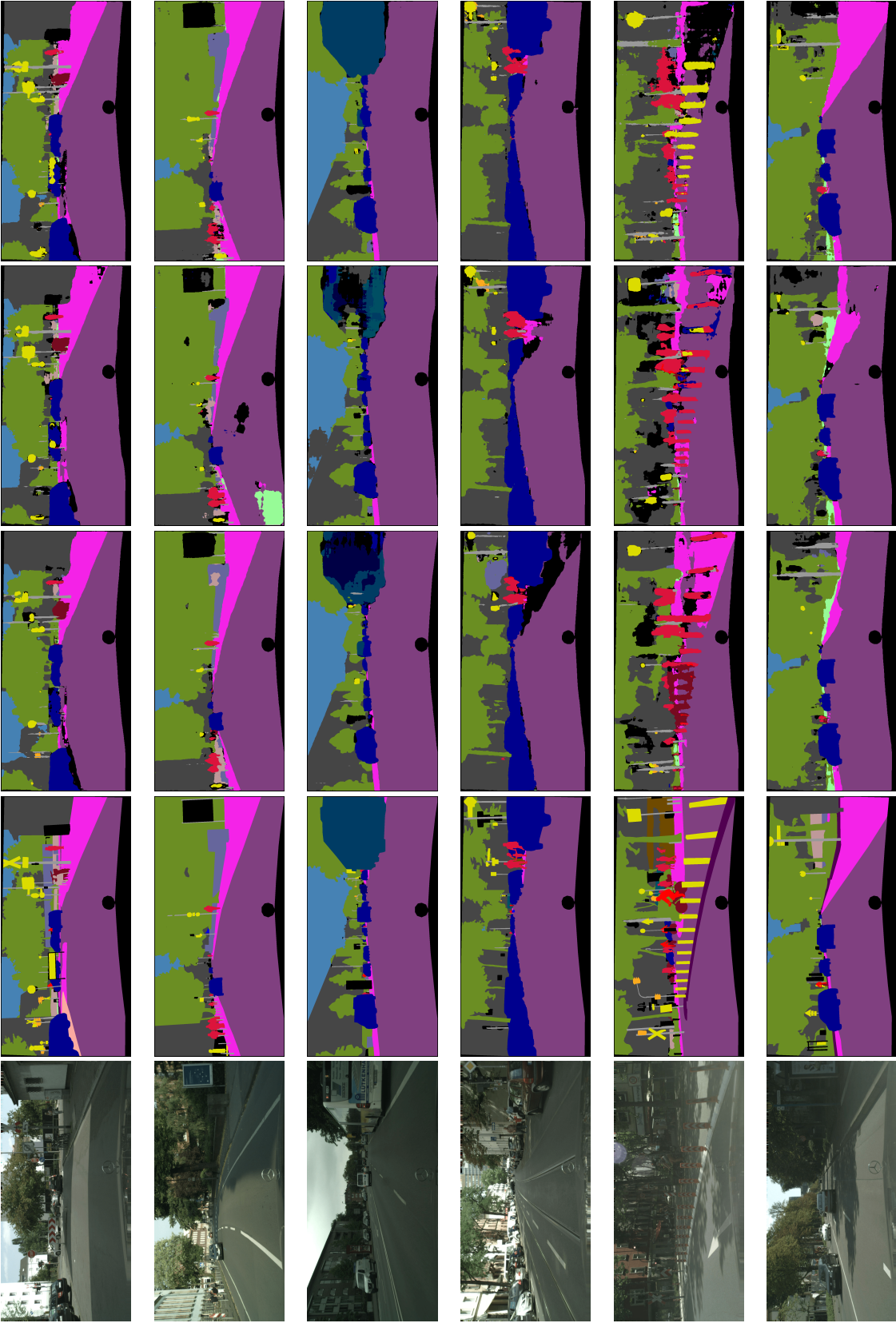


Figure 8: Qualitative results of Cityscapes baseline experiments (from the left– input image, ground truth, HRNet-V2, U-Net, and PDFNet12 )

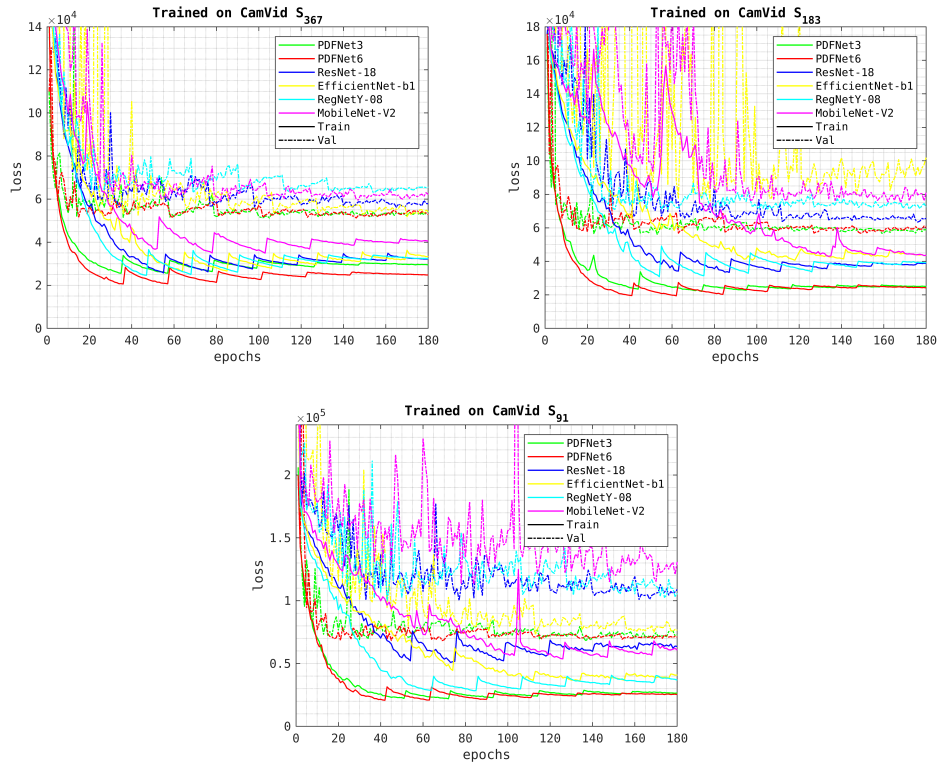


Figure 9: CamVid set-1 training plots

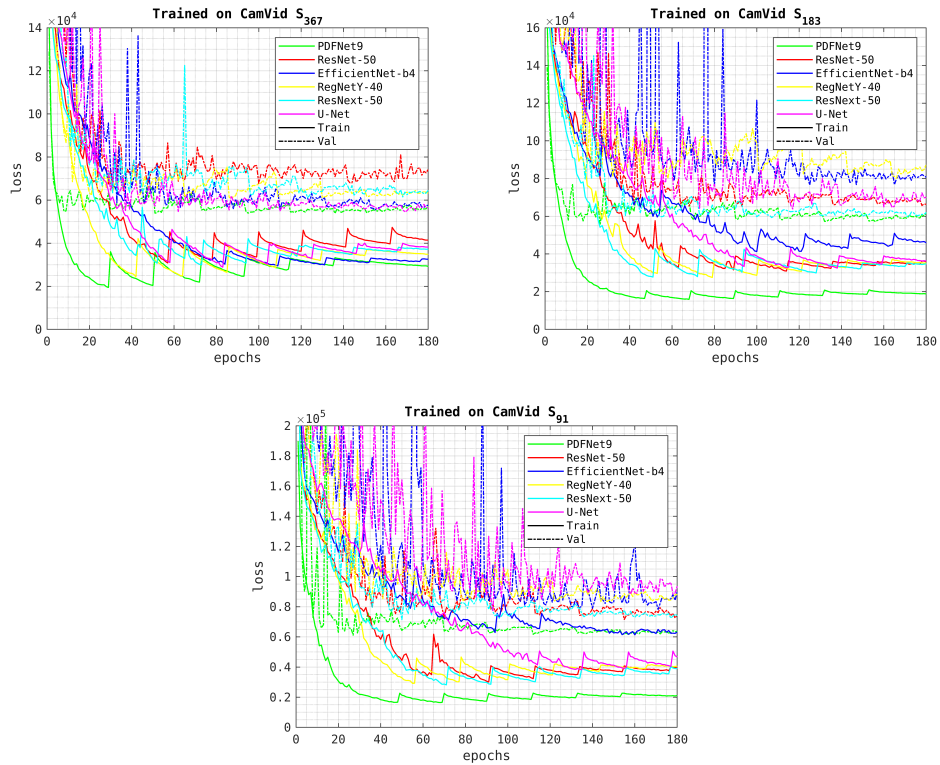


Figure 10: CamVid set-2 training plots

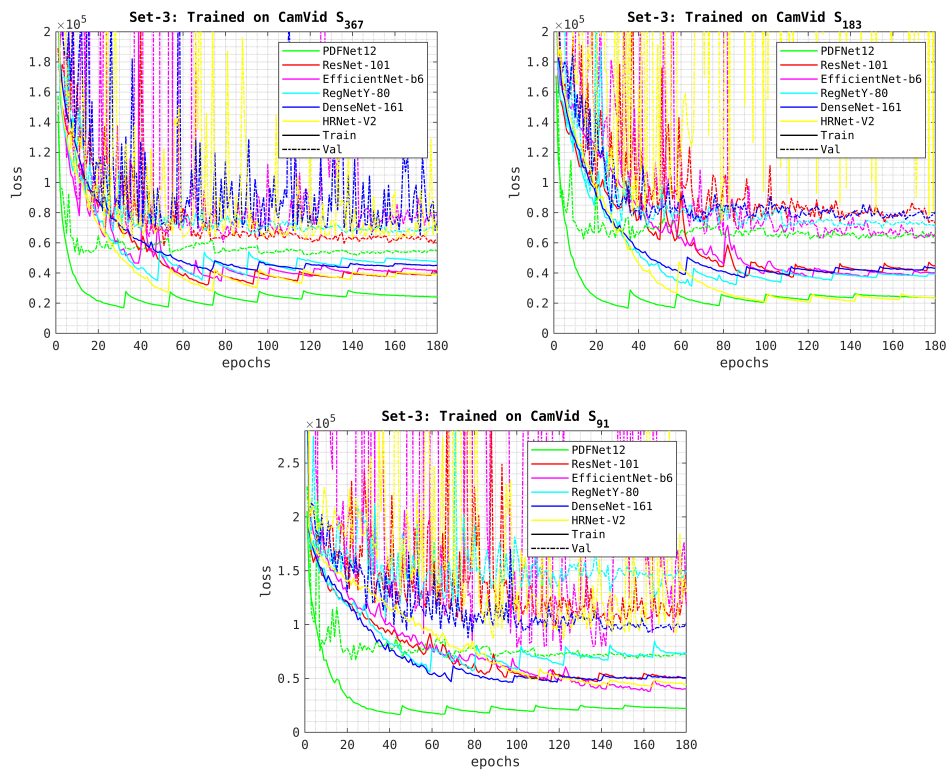


Figure 11: CamVid set-3 training plots